Norwegian University of Life Sciences

Master's Thesis 2024 60 ECTS

Faculty of Chemistry, Biotechnology and Food Sciences

Investigating the inflammatory effect of mitochondrial DNA (mtDNA) during sepsis

Emma Lillebø

Master of Science, Biotechnology

Investigating the inflammatory effect of mitochondrial DNA (mtDNA) during sepsis

Oslo University Hospital,
Department of Medical Biochemistry

And

Norwegian University of Life Science (NMBU),
Faculty of Chemistry, Biotechnology and Food Sciences

ACKNOWLEDGEMENTS

Completing this master's thesis, I have achieved my degree in Biotechnology at the Faculty of Chemistry, Biotechnology, and Food Science at the Norwegian University of Life Science (NMBU). The laboratory work was conducted at the Department of Clinical Biomedicine, Oslo University Hospital Rikshospitalet, from August 2023 to May 2024.

I want to thank my supervisors, Lars Eide and Bjørn Dalhus, for their outstanding support and active involvement in this fascinating project. I am sincerely thankful to both of you for your invaluable guidance and encouragement throughout my master's thesis journey. Thank you for providing me with your insightful feedback and for critically reading my thesis. I appreciate your efforts and valuable input. Lars, your patience, academic skills, and cell biology expertise have contributed to my understanding of the research field. Bjørn, I appreciate your assistance with protein production and related methods and sharing your expertise in this area. Both of you have been incredible mentors, and I am profoundly grateful for everything, as your guidance has not only shaped my research but also my personal and professional growth.

I want to thank Marte Eikenes, Pernille Blicher, Viktoria Holsvik, and Georgina Fura Munoz for contributing to my lab work. Marte and Pernille, thank you for your assistance with the lab methods and your patience in explaining even the simplest things. I am also grateful for our enjoyable conversations during the lab work, which made my days brighter. Viktoria and Georgina, I appreciate your constant cheerfulness and supportive words during the challenging times in the lab. Your positive attitude, smiles, laughter, and acts of kindness made every day in the lab enjoyable. You have all made my overall experience more enjoyable than I could have ever imagined. I would also like to thank everyone at IKB for good conversations in the lunch breaks.

Finally, I would like to thank my family for their support. Ida, in particular, deserves a special mention for always being there to listen to me and discuss my results. My friends also played a crucial role in helping me stay motivated and focused by accompanying me on café visits to discuss the writing process. I would also like to thank the people at Oslo Powerlifting Club for providing me with valuable breaks from my studies and helping me improve my physical and mental strength.

Ås, May 2024

Emma Lillebø

ABSTRACT

Sepsis is a life-threatening condition that is a worldwide health liability. Sepsis occurs when the body's immune system becomes dysregulated, causing multiple organ failure and potentially resulting in death. Detecting the disease in its early stages and receiving timely treatment can significantly improve patient outcomes and increase chances of survival. Thus, effective biomarkers are necessary to detect sepsis in its early stages. Understanding the origin and mechanism of sepsis is crucial for developing sufficient biomarkers.

The Cyclic GMP-AMP synthase (cGAS) plays a critical role in our immune response by identifying cytosolic DNA and initiating a series of events. When cytosolic DNA binds to cGAS, it triggers the synthesis of cyclic GMP-AMP (cGAMP), which is a second messenger that activates the stimulator of interferon genes (STING) pathway. This signaling cascade is not only essential for our defense against viral and bacterial infections, but it is also vital for recognizing abnormal self-DNA. The dysregulation of the cGAS-STING pathway has been implicated in the pathogenesis of various autoimmune and inflammatory disorders. Therefore, this master project aims to better understand the cGAS activation pathway in the development and progression of sepsis, and the potential involvement of mitochondrial DNA (mtDNA) and possibly other nucleic acids, in extracellular vesicles (EVs) and plasma. The study assessed the affinity between cGAS and various nucleic acids through microscale thermophoresis (MST). To estimate cGAS activation across different cohorts—sepsis patients, organ failure patients, and healthy controls—the production of cGAMP was quantified via enzyme-linked immunosorbent assay (ELISA). Furthermore, to determine the role of RNA in this activation process, patient samples were pre-treated with RNase before cGAMP quantification. Finally, quantitative polymerase chain reaction (qPCR) was employed to estimate the levels of nuclear DNA (nDNA), mitochondrial DNA (mtDNA), and mtDNA damage in the patient samples.

The study discovered some unanticipated differences between the binding of cGAS and the production of cGAMP, particularly regarding RNA-DNA hybrids. The activation of cGAS was higher in plasma samples than in EV samples, with RNase significantly affecting cGAS activation in both sample types. Further, the control groups of plasma exhibited higher levels of cGAS-activation than the sepsis and organ failure groups. Furthermore, plasma contained more mtDNA, while EVs had a higher prevalence of damaged mtDNA. Compared to controls, plasma from the sepsis and organ failure groups had significantly elevated nDNA levels.

SAMMENDRAG

Sepsis er en livstruende tilstand som utgjør en global helsebyrde. Sepsis oppstår når kroppens immunsystem blir dysregulert, dette forårsaker multiorgansvikt som kan føre til død. Å oppdage sykdommen i tidlige stadier og rask starte behandling kan betydelig forbedre pasientresultater og øke sjansene for overlevelse. Effektive biomarkører er nødvendige for å oppdage sepsis tidlig. Forståelse av opprinnelsen og mekanismen til sepsis er avgjørende for å utvikle gode biomarkører.

Den sykliske GMP-AMP-syntasen (cGAS) spiller en kritisk rolle i vårt immunforsvar ved å identifisere cytosolisk DNA og igangsette en rekke hendelser. Når cytosolisk DNA binder seg til cGAS, utløser det syntesen av syklisk GMP-AMP (cGAMP), som er en sekundærmessenger som aktiverer stimulatoren av interferongener (STING) -veien. Denne signalveikaskaden er ikke bare essensiell for vårt forsvar mot virale og bakterielle infeksjoner, men den er også vital for å gjenkjenne unormalt selv-DNA. Dysreguleringen av cGAS-STING-veien har blitt knyttet til patogenesen av ulike autoimmune og inflammatoriske lidelser. Derfor har denne masteroppgaven som mål å bedre forstå cGAS-aktiveringsveien i utviklingen og progresjonen av sepsis og den potensielle involveringen av mitokondrielt DNA (mtDNA) og muligens andre nukleinsyrer, i extracellulære vesikler (EV) og plasma. Studien vurderte affiniteten mellom cGAS og ulike nukleinsyrer gjennom mikroskala termoforese (MST). For å estimere cGAS-aktivering på tvers av ulike grupper – sepsis-pasienter, pasienter med organsvikt og friske kontroller – ble produksjonen av cGAMP kvantifisert via enzymkoblet immunosorbentanalyse (ELISA). Videre, for å bestemme rollen til RNA i denne aktiveringsprosessen, ble pasientprøver behandlet med RNase før kvantifisering av cGAMP. Til slutt ble kvantitativ polymerasekjedereaksjon (qPCR) brukt for å estimere nivåene av nukleært DNA (nDNA), mitokondrielt DNA (mtDNA) og mtDNA-skade i pasientprøvene.

Studien oppdaget noen uventede forskjeller mellom bindingen av cGAS og produksjonen av cGAMP, spesielt med hensyn til RNA-DNA-hybrider. Aktiveringen av cGAS var høyere i plasmaprøver enn i EV-prøver, og RNase påvirket cGAS-aktivering betydelig i begge prøvetypene. Videre viste kontrollgruppene av plasma høyere nivåer av cGAS-aktivering enn sepsis- og organsviktgruppene. Plasma inneholdt mer mtDNA, mens EV hadde en høyere forekomst av skadet mtDNA. Sammenlignet med kontroll gruppen viste plasma fra sepsis- og organsviktgruppene signifikant forhøyede nivåer av nDNA.

ABBREVIATIONS

2'3'-cGAMP	2'3'-cyclic GMP-AMP
AIM2	Absent in melanoma 2
AMP	Adenosine monophosphate
apDNA	Apurinic/apyrimidinic DNA
ATP	Adenosine triphosphate
B_0	Maximum binding
Blk	Blank
bp	Basepairs
Buffer AE	Elution buffer
Buffer AL	Lysis buffer
Buffer AW	Wash buffer
B/B_0	Standard bound/maximum bound
cGAS	Cyclic GMP-AMP synthase
C_T	Cycle Threshold
DC	Dendritic cell
DMSO	Dimethyl Sulfoxide
DNA	Deoxyribonucleic acid
dsDNA	Double-stranded DNA
dsRNA	Double-stranded RNA
ED	Emergency department
ELISA	Enzyme-linked immunosorbent assay
EVs	Extracellular vesicles
E. coli	*Escherichia coli*
FAM	Fluorescein
FP	Fusion protein
G	Glycerol
GMP	Guanosine monophosphate
GTP	Guanosine triphosphate
hcGAS	Human cGAS
His-tag	Histidine-tag
HIV1	Human Immunodeficiency Virus type 1

HRP	Horseradish Peroxidase
IFNs	Interferons
IgG	Immunoglobulin G
IMAC	Immobilized metal affinity chromatography
IPTG	Isopropyl-β-D-1-thiogalactopyranoside
IRF3	Interferon regulatory factor 3
ISD	Interferon-stimulatory DNA
K_D	Equilibrium dissociation constant
kDa	Kilodalton
LED	Light emitting diode
ln	Natural logarithm
Mab21	Male abnormal gene family 21
mcGAS	Mouse cGAS
mmDNA	Mismatch DNA
MOPS	3-(N-morpholino) propane sulfonic acid
MPa	Megapascal
MST	Microscale thermophoresis
mtDNA	Mitochondrial DNA
Ni^{2+}	Nickel
nDNA	Nuclear DNA
NLRP	NOD-like receptor family pyrin domain-containing protein
NOD	Nucleotide-binding oligomerization domain
NSB	Non-specific binding
NTA	Nitrilotriacetic acid
Ntase	Nucleotidyltransferase
OD_{600}	Optical density at 600 nm
OUS	Oslo Universitetssykehus
PBS	Phosphate-Buffered Saline
PRRs	Pattern recognition receptors
qPCR	Quantitative polymerase chain reaction
REK	Regionale komiteer for medisinsk og helsefaglig forskningsetikk
RNA	Ribonucleic acid
SD	Standard deviation

SDS-PAGE	Sodium dodecyl sulfate-polyacrylamide gel electrophoresis
SEC	Size-exclusion chromatography
ssDNA	Single-stranded DNA
ssRNA	Single-stranded RNA
STING	Stimulator of interferon genes
SUMO	Small ubiquitin-like modifier
TA	Total activity
TBK1	TANK-binding kinase
TEV	Tobacco etch virus
TLRs	Toll-like receptors
TMB	3,3´,5,5´-tetramethylbenzidine
TP	Truncated protein
uDNA	Uracil-DNA

TABLE OF CONTENTS

1 INTRODUCTION

1.1 SEPSIS

Sepsis is a life-threatening condition that occurs when the body's response to infection becomes dysregulated, leading to organ failure with a high risk of death. Sepsis can result from various infections, such as genitourinary (Porat et al., 2024), respiratory, gastrointestinal, skin, and soft tissue infections. Diagnosing sepsis can be challenging, especially in older individuals and those with weakened immune systems, as symptoms may be subtle. Laboratory tests, including imaging studies, and the measurement of sepsis biomarkers such as procalcitonin and lactate levels, are essential for the initial evaluation. Despite advances in medical knowledge and treatment protocols, sepsis continues to present a significant global health burden. Efforts are being made to improve the quality of life for individuals who survive sepsis by enhancing long-term outcomes (Gauer et al., 2020).

1.1.1 THE IMPORTANCE OF EARLY DETECTION

Detecting sepsis at an early state is crucial, given its involvement in one out of every two to three hospital deaths, often with patients already affected upon admission (Liu et al., 2014). This underscores the urgency of early identification and treatment. Providing consistent care for patients with milder forms of sepsis could lead to decreased mortality rates in the future. Singer et al. (2016) present updated definitions and clinical criteria, emphasizing the timely management of sepsis patients or those at risk. Recognizing the body's dysfunctional response to infection and organ failure, indicative of sepsis, is crucial. Early detection facilitates rapid intervention and improves outcomes, underscoring its significance in enhancing patient recovery and reducing mortality rates associated with sepsis.

1.1.2 INFLAMMATION AND SEPSIS

To understand the role of inflammation in sepsis, it is essential to understand what inflammation is and how it affects physiological and pathological processes, particularly infections. In response to harmful stimuli like infections or tissue damage, our body initiates an inflammatory response as a protective mechanism (Medzhitov, 2008). Inflammation is a complex biological process that involves activation of various molecules and cells, such as dendritic cells (DCs),

through signals generated by stressed or infected cells (Gallucci et al., 1999). DCs play a crucial role in initiating immune responses, and the type of signal received can determine the nature of the response. An unregulated inflammatory response in sepsis results from a severe infection, leading to tissue damage and organ failure (Gustot, 2011). Understanding the mechanisms underlying inflammation in sepsis to develop effective therapies are crucial.

1.2 EXTRACELLULAR VESICLES AND CIRCULATION IN SEPSIS

Extracellular vesicles (EVs) are tiny membrane-bound particles that cells release into the extracellular space. These particles facilitate communication between cells and transfer crucial biological information. There are three distinct types of extracellular vesicles: exosomes, microvesicles, and apoptotic bodies, each originating from different cellular mechanisms (Yanez-Mo et al., 2015). Exosomes are formed from the inward budding of endosomal membranes, while microvesicles result from outward plasma membrane budding. Apoptotic bodies are generated when cells undergo apoptosis. EVs play a critical role in intercellular signaling, essential for various physiological and pathological processes such as cancer, neurodegenerative diseases, and immune modulation. EVs from patients with septic shock contain molecular components related to inflammatory response, oxidative stress, and cell cycle regulation (Real et al., 2018).

1.2.1 EVS IN CELL COMMUNICATION

EVs are essential in facilitating communication between cells. These vesicles are released by various cell types, including immune, mesenchymal, and cancer cells (Kahlert & Kalluri, 2013). EVs contain various molecular components, such as proteins (Vagner et al., 2019), RNA (Hunter et al., 2008), and DNA (Kahlert et al., 2014), such as mitochondrial DNA (mtDNA) (Lazo et al., 2021). They can interact with recipient cells by fusing their membranes or transferring their contents, activating signaling pathways, and influencing cellular behavior (Kalluri, 2016). The heterogeneity of EVs reflects the phenotypic state of the cells that release them, and their dynamic nature allows for the transmission of specific information between cells (Kowal et al., 2016). Overall, EVs play a critical role in cell-to-cell communication, which has significant implications for various physiological and pathological processes.

1.2.2 Inflammation and DNA

DNA plays a crucial role in inflammation and the development of sepsis. Microbial infections, such as those caused by bacteria, viruses, and fungi, release DNA into cells, triggering an inflammatory response (Das, 2023). Circulating cell-free DNA, particularly mtDNA, is closely associated with inflammation and organ dysfunction in sepsis. Several studies have shown that increased level of mtDNA in the bloodstream is linked with higher mortality rates among sepsis patients, as suggested by the work of Krychtiuk et al. (2015) and Sursal et al. (2013). For instance, a recent study conducted by Wang et al. (2020) discovered that higher plasma mtDNA levels were associated with a poor prognosis of sepsis and could serve as a predictor of 28-day mortality. The research also demonstrated that plasma mtDNA levels, lactate concentration, and their combined variable showed predictive value for sepsis outcomes. These findings highlight the potential usefulness of mtDNA as a biomarker for predicting sepsis outcomes. They could have valuable implications for developing new treatments for this life-threatening condition.

1.2.2.1 mtDNA as a danger signal

mtDNA may be associated with bacteria because of its evolutionary origin. This similarity may explain the human innate immune system's ability to identify mtDNA as a potent danger signal, which can directly impact the inflammatory response. Understanding the resemblance between mtDNA and pathogenic DNA is critical in comprehending its function as a pathogenic factor in various inflammatory diseases. Moreover, this resemblance presents new opportunities to target mtDNA-mediated inflammation in different human inflammatory diseases (Boyapati et al., 2017).

1.3 Circulating DNA: A potent inflammatory mediator

Circulating DNA, particularly nuclear (nDNA) and mtDNA, are significant indicators of sepsis mortality (Timmermans et al., 2016). During sepsis, both nDNA and mtDNA are found in the bloodstream. These nucleic acids can bind to pattern recognition receptors (PRRs), which can produce inflammatory cytokines that contribute to the initiation and propagation of inflammation. Additionally, the levels of nDNA and mtDNA in the bloodstream are associated with inflammation markers, shock severity, and organ damage in cases of septic shock. Therefore, nDNA and mtDNA could provide valuable insight into the pathophysiology of sepsis and act as biomarkers for predicting patient outcomes (Kaczmarek et al., 2013).

1.3.1 mtDNA

mtDNA is present within the mitochondria of every eukaryotic cell except for erythrocytes. It is a double-stranded circular DNA of approximately 16.6 kb that encodes genes necessary for respiratory chain complexes that are essential for energy production (Anderson et al., 1981; Habbane et al., 2021). While nDNA is inherited from both parents, mtDNA is only inherited from the mother (Giles et al., 1980). Mutations in mtDNA can cause various mitochondrial disorders, affecting multiple body organs and tissues (Wallace & Chalkia, 2013).

1.3.2 Mechanisms of mtDNA release and recognition

mtDNA can be released outside the organelle, and potentially outside the cell, under certain conditions, such as cellular damage or stress. Cell-free mtDNA, or mtDNA in extracellular vesicles (EVs), can also be taken up by cells through endocytosis (Morelli et al., 2004). Some proteins, such as Toll-like receptor 9 (TLR9), recognize hypomethylated CpG motifs in DNA (West & Shadel, 2017), and they are crucial in identifying mtDNA and triggering an immune response (Kim et al., 2023). This immune response can lead to inflammation and release harmful chemicals in the body. The immune system senses mtDNA as a danger signal, indicating something is wrong. These processes can contribute to developing sepsis and other inflammatory responses in the body (Di Caro et al., 2016).

1.3.3 mtDNA receptors

mtDNA can be recognized by several different recognition receptors, leading to the activation of various signaling pathways involved in the inflammatory response. TLRs, specifically TLR9, play an essential role in the immune system by recognizing specific patterns associated with pathogens (PRRs) and initiating an immune response (Garcia-Martinez et al., 2016). Other receptors, such as Nucleotide-binding oligomerization domain (NOD)-like receptor family pyrin domain-containing proteins (NLRP1, NLRP3 and NLRC4) and Absent in melanoma 2 (AIM2), detect danger signals inside our cells and activate an inflammatory response (Man & Kanneganti, 2016). These receptors are part of a multiprotein machinery called the inflammasome, mainly found in immune cells like macrophages. Another pathway in the immune system, called the cGAS-STING DNA-sensing system, also detects mitochondrial DNA and other cytosolic DNA that trigger the production of interferons and cytokines (Mankan et al., 2014). **Figure 1.1** illustrates various ways in which mtDNA can induce inflammation.

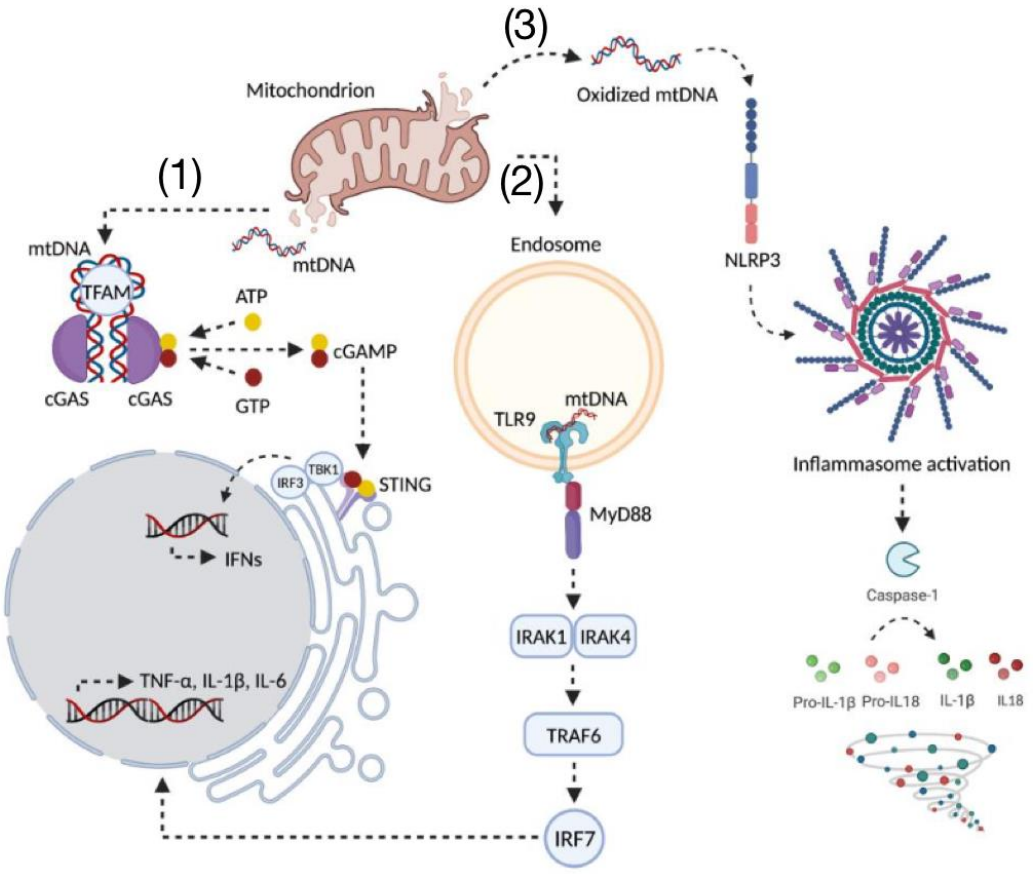

Figure 1.1: Illustration describing the essential pathways involved in inflammation triggered by the displacement of mitochondrial components. *Displaced mitochondrial-derived components, such as mtDNA, can be recognized as damage associated molecular patterns and trigger inflammation by activating three distinct signaling pathways via the interaction with* ***1)*** *cytosolic cGAS-STING DNA-sensing system;* ***2)*** *Toll-like receptors (TLRs); and* ***3)*** *NOD-like receptor family pyrin domain-containing protein 3 (NLRP3) inflammasome. Illustration adapted from Picca et al. (2022).*

1.4 Cyclic GMP- AMP synthase

Cyclic Guanosine monophosphate (GMP)- Adenosine monophosphate (AMP) synthase (cGAS) is a 60 kDa protein with a non-conserved amino-terminal stretch composed of approximately 130–150 residues, along with a highly conserved male abnormal gene family 21 (Mab21) domain belonging to the nucleotidyltransferase (NTase) superfamily (Zhou et al., 2023). cGAS functions as a cytosolic DNA sensor; thus, its activation is determined by its recognition of cytosolic double-stranded DNA (dsDNA). cGAS can be activated by dsDNA from multiple sources, such as microbial DNA, mtDNA, nuclear chromatin, extracellular self-DNA, cytosolic chromatin, micronuclei, and dysfunctional telomeres (Herzner et al., 2015).

The dsDNA from microbes can enter the cytosol and be sensed by cGAS, leading to a downstream signaling cascade. After identifying specific DNA stimulants in mammalian cells, DNA binds to two locations on the catalytic domains of the cGAS (Li et al., 2013). This results in a 2:2 cGAS-dsDNA complex oriented in two directions, as shown in **Figure 1.2**. This complex represents the smallest active enzymatic unit (Decout et al., 2021). Additionally, in the human cGAS (hcGAS), the 2:2 cGAS–dsDNA complexes rearrange themselves to create a ladder-like network that enables the successive recruitment of adjacent cGAS to form more 2:2 cGAS–dsDNA and stabilize its structure (Zhou et al., 2018).

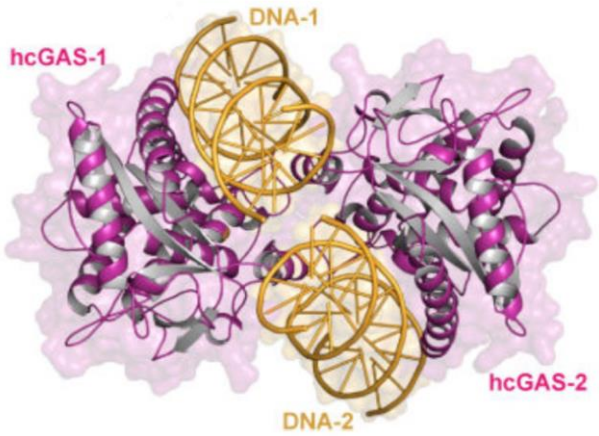

Figure 1.2: Schematic overview of 2:2 cGAS-dsDNA complex. *hcGAS forms a 2:2 complex with DNA where each cGAS monomer has two distinct DNA-binding surfaces (Zhou et al., 2018).*

1.4.1 cGAS ENZYMATIC ACTIVITY

cGAS is a cytosolic DNA sensor in mammalian cells, that activates the immune system by catalyzing the synthesis of a second messenger, cyclic GMP-AMP (cGAMP), from cytosolic adenosine triphosphate (ATP) and guanosine triphosphate (GTP) (Sun et al., 2013). cGAMP then binds to a protein, stimulator of interferon genes (STING), which triggers downstream signaling events, such as the recruitment of TANK-binding kinase 1 (TBK1) (Hu et al., 2018) and the phosphorylation of the transcription factor interferon regulatory factor 3 (IRF3), which induces the production of type I interferons (IFNs) and other inflammatory mediators (Decout et al., 2021; Liu et al., 2015). Overall, the cGAS-mediated DNA detection results in the activation of immune responses against pathogens and cellular stress (illustrated in **Figure 1.3**).

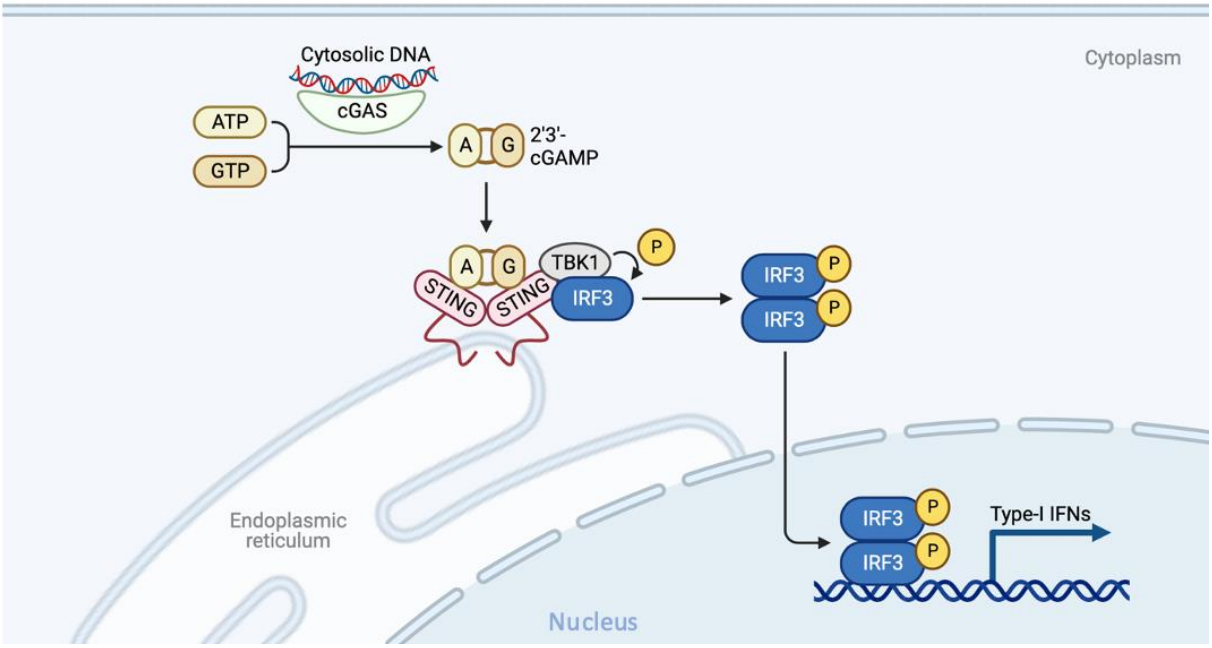

Figure 1.3: Overview of the cGAS-STING signaling pathway. *Illustration of the way cGAS-DNA interaction leads to the production of cGAMP from ATP and GTP. cGAMP then binds to STING, which recruits TBK1. TBK1 phosphorylates and activates IRF3 which promotes the production of type- I IFNs. Figure created by Biorender.com.*

1.4.2 cGAS-NUCLEIC ACID BINDING

The cGAS enzyme responds to various types of DNA in a length-dependent manner. Luecke et al. (2017) found that the ability of DNA to activate cGAS depends on their concentration and length. Long DNA molecules can efficiently activate cGAS at low concentrations, while short DNA strands require high concentrations to induce a strong response. dsDNA longer than 40 base pairs is required to activate cGAS (Herzner et al., 2015).

Some nucleic acid types that activate cGAS include dsDNA, circular DNA, RNA-DNA hybrids (Mankan et al., 2014), and mtDNA (as shown in **Figure 1.4**). In addition, L. Wang et al. (2022) highlighted that cGAS activation was increased by damaged DNA as compared to intact DNA. Longer and more flexible DNA sequences are more effective at activating cGAS. However, some shorter DNA fragments can activate cGAS as well if they have specific structures or sequences. For instance, the "stem-loop" structure formed during the reverse transcription of Human Immunodeficiency Virus type 1 (HIV1) can activate cGAS in a sequence-dependent manner, even though it is relatively short in length. There is also phylogenetic differences; according to Zhou et al. (2018), the hcGAS enzyme synthesizes 2′3′-cGAMP when exposed to increasing amounts of 45 basepairs (bp) DNA but remains inactive if the DNA is only 17 bp

long. However, the mouse cGAS (mcGAS) enzyme recognizes DNA with similar efficiency, regardless of whether it is 45 bp or 17 bp long. The human-specific substitutions in hcGAS, K187N, and L195R, making it more similar to the mcGAS, allow it to identify and activate in the presence of 17 bp DNA, improving immune surveillance.

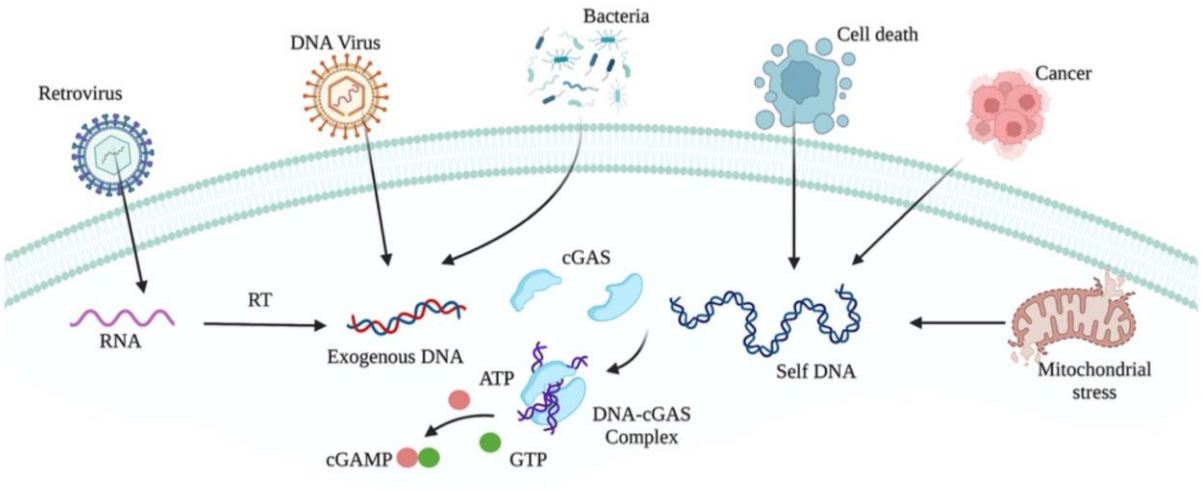

Figure 1.4: Illustration showing various origins of nucleic acids that can be detected by cGAS. *cGAS can detect both exogenous nucleic acids from viruses and bacteria, and self-DNA released due to cellular stress. Illustration adapted from D. Wang et al. (2022).*

2 AIMS OF THE THESIS

This thesis is a pilot study that aims to investigate the putative role of mtDNA and cGAS activation in the pathogenesis of sepsis. Sepsis is a life-threatening condition that arises due to a dysregulated host response to infection (Singer et al., 2016). Recent research has shown that mtDNA can activate the immune system through various signaling pathways (Nakahira et al., 2011) including the cGAS-STING pathway (Decout et al., 2021), which may contribute to the development and progression of sepsis.

This study's primary hypothesis proposes that cGAS undergoes hyperactivation during sepsis due to the status and levels of mtDNA in circulation, leading to a dysregulated immune response. To investigate this hypothesis, the first aim was to characterize cGAS binding to defined substrates (synthetic oligonucleotides), followed by the second aim to interpret activation induced by synthetic oligonucleotides and isolated nucleic acids from human material. Finally, the study also aimed to characterize nucleic acids typical of sepsis.

These aims were addressed through the following objectives:

- Expression and purification of human cGAS for *in vitro* cGAMP synthesis.

- Determining cGAS binding affinity to different oligonucleotides using microscale thermophoresis (MST).

- Determining the cGAS activation through quantifying cGAMP production by enzyme-linked immunosorbent assay (ELISA).

- Characterization of nucleic acids from human sepsis patients, using two control groups: patients with organ failure but not sepsis, and healthy controls.

3 MATERIALS AND METHODS

3.1 HUMAN MATERIAL

This research project involved different types of human material: citrated plasma, EDTA plasma, and isolated EVs. There were healthy control samples, from non-fasted and fasted for 12 hrs, and samples from patients with sepsis or organ dysfunction, and patients with rare, inborn disease of metabolism. Both sample types included healthy controls and sepsis patients, listed in detail in Appendix A. The EVs were kindly provided by a collaborating group at Oslo Universitetssykehus (OUS) using Size-exclusion chromatography (SEC). After SEC isolation, the EVs' mean size was approximately 120 nm, with a mode size of around 100 nm. The samples were stored in the freezer at -20°C.

3.1.1 REK APPROVAL FOR BIOMEDICAL RESEARCH

OUSs Sepsis Quality Register is an authorized database by the Regional Committees for Medical and Health Research Ethics (REK 2017/19067) that keeps track of all suspected sepsis cases in the Emergency Department (ED) at OUS and quickly responds to them with a rapid response team. As of August 2021, the Register has recorded over 2 200 admissions, which includes detailed clinical information, 30-day outcomes, and retrospective evaluations of the probability of infection and the onset of organ dysfunction. Since January 2020, the sepsis biobank (REK 2019/306) has acquired samples from 450 patients.

There are three projects/biobanks associated with the controls in this project. The first project, REK 2017/2189, aims to establish reference ranges in normal individuals, for branched fatty acids and mtDNA. This project is valid to October 31, 2025. The second biobank, REK 2017/2217, stores "Plasma reference material" and contains fasting and non-fasting samples from healthy controls. Lastly, the third biobank, REK 2017/2218, "Rare metabolic disorders," stores plasma samples from patients with rare metabolic disorders.

3.2 PROTEIN EXPRESSION AND PURIFICATION

The expression and purification steps were performed using a protocol developed in this project.

3.2.1 PROTEIN EXPRESSION

cGAS was expressed and purified using BL21-OneShot (DE3) *E. coli* cells (Agilent Technologies). The *E. coli* bacteria were transformed with a kanamycin-resistant pET-SUMO cGAS vector that contained an N-terminal hexa histidine tag (His-tag), followed by a small ubiquitin-like modifying protein (SUMO) tag and a Tobacco Etch Virus (TEV) cleavage site. This vector (illustrated in **Figure 3.1)** allowed for good solubility and a simplified purification process. The cGAS sequence contained residues 157-522 of human cGAS (Uniprot Entry Q8N884).

MGSSHHHHHHGSGLVPRGSASMSDSEVNQEAKPEVKPEVKPETHINLKVSDGSSEIFFKIKKTTPLRRLMEAFAK
RQGKEMDSLRFLYDGIRIQADQTPEDLDMEDNDIIEAHREQIGGGGLENLYFQGGDAAPGASKLRAVLEKLKLSR
DDISTAAGMVKGVVDHLLLRLKCDSAFRGVGLLNTGSYYEHVKISAPNEFDVMFKLEVPRIQLEEYSNTRAYYFV
KFKRNPKENPLSQFLEGEILSASKMLSKFRKIIKEEINDIKDTDVIMKRKRGGSPAVTLLISEKISVDITLALES
KSSWPASTQEGLRIQNWLSAKVRKQLRLKPFYLVPKHAKEGNGFQEETWRLSFSHIEKEILNNHGKSKTCCENKE
EKCCRKDCLKLMKYLLEQLKERFKDKKHLDKFSSYHVKTAFFHVCTQNPQDSQWDRKDLGLCFDNCVTYFLQCLR
TEKLENYFIPEFNLFSSNLIDKRSKEFLTKQIEYERNNEFPVFDEF

Figure 3.1: cGAS-SUMO fusion protein amino acid sequence. *The amino acids colored orange demonstrates the 6xHis-tag; blue shows the amino acid sequence of the SUMO protein; red is the TEV protease cleavage site, and green shows the residues 157-522 of human cGAS.*

To initiate bacterial culture for protein expression, 10 mg of kanamycin (Sigma-Aldrich) was added to 100 mL of Luria Broth (LB) medium (Oslo University Hospital). This medium was further inoculated with a small sample of transformed *E. coli* cells, stored at -80°C in glycerol. The mixture was incubated overnight in a 311DS shaking incubator (Labnet International) at 150 rpm and 37°C. A larger cell culture, a 1:100-fold dilution of the overnight culture, was then created by adding 10 mL of the overnight culture to 1 L autoclaved LB medium [25 g LB-broth powder per 1 L Milli-Q H_2O] (Invitrogen™, Merck Millipore) supplemented with 100 mg kanamycin. This new mixture was incubated in a Multitron incubator rotary shaker (Infors HT) at 180 rpm and 37°C until reaching an optical density of approximately 0.5 at 600 nm (OD_{600}). The temperature in the shaker was then reduced from 37°C to 18°C. After one hour of incubation at 18°C, 1 mL of 0.25 M isopropyl-β-D-1-thiogalactopyranoside (IPTG) (Apollo

Scientific) was added to the cell culture to initiate enzyme expression (Gomes et al., 2020). The cell culture was incubated overnight at 18°C and 180 rpm. Next, the cell culture underwent centrifugation at 5 000 rpm for 20 minutes at 15°C in a Sorvall Lynx 6.000 centrifuge (Thermo Scientific™) with a Fiberlite F9- 6x1.000 Lex angle rotor (Thermo Scientific™).

3.2.2 PROTEIN ISOLATION AND PURIFICATION

3.2.2.1 Sonication

The protein was extracted by lysing cells with sonication. The cell pellet acquired from centrifugation was dissolved and homogenized in 15 mL of buffer A [300 mM NaCl, 50 mM Tris pH 8.0, 10 mM imidazole]. To extract proteins, sonication was employed as a method to disrupt the cell membrane using high-energy shockwaves (Ferdous et al., 2021). Using a Vibra Cell Sonicator (Sonics & Materials Inc.), sonication with an amplitude of 60 for a duration of 30 seconds was performed three times with pauses on ice lasting for one minute between each interval. These intervals were crucial in maintaining a low temperature and preventing enzyme degradation. Once sonication was completed, the sonicated *E.coli* cells underwent centrifugation with a Fiberlite F21-8x50y angle rotor (Thermo Scientific™) at 15 000 rpm at 4°C for half an hour leading to the separation of supernatant comprising soluble proteins and nucleic acids. The resulting supernatant was kept on ice until the purification process started.

3.2.2.2 Immobilized metal affinity chromatography

Recombinant 6xHis-tagged cGAS was purified by Immobilized Metal Affinity Chromatography (IMAC). Nickel (Ni^{2+}) was the immobilized metal on agarose beads within a column. These metal ions, coupled to a compound called nitrilotriacetic acid (NTA), firmly adhere to the beads. When introducing proteins with histidine tags into the column, these proteins selectively bind to the immobilized nickel ions due to the robust affinity between histidine residues and nickel ions. This specific binding enables the selective capture of the target protein while other proteins and impurities are effectively washed away. Subsequent release of the targeted protein from the column is achieved using a buffer solution with imidazole, which competes with the histidine residues for binding to the metal ions (He et al., 2015).

As preparation for the IMAC purification step, 2 mL Nickel NTA agarose (GoldBio) per 1 L cell culture was added to a 50 mL Falcon tube, which was then filled with Milli-Q water. After centrifugation for 10 minutes, the supernatant was discarded, and the washing process was repeated to eliminate any residual ethanol from the Ni^{2+}-resin solution. The supernatant from the cell culture centrifugation was combined with the Ni^{2+}-NTA agarose and incubated for at least 15 minutes at 4°C with a rocking motion to facilitate the binding of His-tagged proteins to the Ni^{2+}-ions.

Following incubation, the Ni^{2+}-NTA solution was loaded onto an Econo column (Bio-Rad). Washing of the Ni^{2+}-resin was carried out using 30 mL of Buffer A, a solution containing 10 mM imidazole. Subsequently, the His-tagged protein, cGAS, was twice eluted in three fractions of 5 mL each. The first elution utilized 15 mL of Buffer B, containing 50 mM imidazole, and the process was repeated with Buffer C, which contained 300 mM imidazole.

The fractions containing the highest protein levels were analyzed on sodium dodecyl sulfate-polyacrylamide gel electrophoresis (SDS-PAGE) and transferred to a Falcon tube equipped with an Amicon® Ultra – 15 Centrifugal Filter (Merck Millipore) with pore size 10 kDa. The sample was centrifuged using a Centrifuge 5702 R (Eppendorf) until reaching a final volume of approximately 500 µL.

3.2.2.3 Size-exclusion chromatography

SEC was utilized to purify the protein further. This technique separates biomolecules by size, using porous particles with a controlled pore size as the stationary phase and an aqueous buffer as the mobile phase (Fekete et al., 2014). A 25mL Enrich SEC 70 column (BioRad) was employed in the process, which was carried out at 10°C, with a flow rate of 0.500 mL/min and a maximum pressure of 2.10 MPa, utilizing an NGC™ Chromatography System (Bio-Rad). The absorbance was monitored at 280 nm.

Before the SEC procedure, the column was washed with 30 mL of Phosphate-Buffered Saline (PBS; OUS). Then, 500 µL of the sample was applied to a 1 mL loop for sample application. The cGAS-SUMO fusion protein was eluted using PBS in 500 µL fractions. To assess sample purity and analyze the fractions with the most protein, SDS-PAGE was conducted with a 12% Bis-Tris plus gel from Invitrogen™ (see section 3.2.2.5).

3.2.2.4 TEV protease cleavage

A His-tagged variant of TEV protease (Produced at the Regional core facility for structure biology, Universitetet i Oslo (UiO) and OUS) was utilized to eliminate the SUMO tag by cleaving the TEV site. For every 30 µL of protein sample, 1 µL of 0.6 mg/ml TEV protease was added. The samples were kept at 4°C for about 48-72 hours. To eliminate any remaining SUMO tag in the samples, 1 µL of Nickel NTA agarose was added per 40 µL of the protein sample. After being incubated with a rocking motion for at least 15 minutes at 4°C, the sample was centrifuged for 10 minutes. The supernatant containing the protein was carefully transferred to a new Eppendorf tube, and the concentration was measured before it was stored on ice for future analyses.

3.2.2.5 Sodium dodecyl sulfate-polyacrylamide gel electrophoresis

To visualize which of the fractions contained the most protein of interest and examine the purity of the samples, SDS-PAGE was used. The proteins were separated based on their molecular mass. The technique involves denaturing the proteins with heat and an anionic detergent, SDS in this case, and subjecting them to electrophoresis through a porous gel matrix (Nowakowski et al., 2014). The SDS binds to the proteins, giving them a negative charge proportional to their molecular mass, allowing for their separation based on size.

5 µL of NuPAGE® LDS Sample buffer (Life Technologies) was combined with 15 µL of the respective fraction and incubated at 70°C for 10 minutes. Subsequently, a 12% Bis-Tris Plus gel was loaded with 10 µL of each prepared sample and 5 µL of SeeBlue® Plus2 Prestained Standard (Invitrogen™), serving as a molecular mass reference ladder. The gel chamber, Novex® Mini-Cell electrophoresis chamber (Invitrogen™), was filled with 3-(N-morpholino) propane sulfonic acid (MOPS) buffer (Invitrogen™) before running SDS-PAGE at 200 volts for 35 minutes using a PowerEase® 90W Power Supply (Life Technologies). Post-electrophoresis, the gel was subjected to Coomassie blue staining [40% methanol, 10% acetic acid, 0.1% Coomassie Blue] for 15 minutes, followed by an overnight destaining process using a destaining solution [40% methanol, 10% acetic acid, and 4% glycerol].

3.2.2.6 Storage

Before storage, the protein concentrations were quantified using a Nanodrop One UV-Vis spectrophotometer (Thermo Scientific^{TM}). The molar extinction coefficient (ε) of 41 990 M^{-1} cm^{-1} was utilized for protein concentration measurement. Four distinct protein versions were stored for subsequent analysis. The cGAS-SUMO fusion protein and cGAS without a SUMO tag were both stored on ice and mixed with 99.5% Glycerol Bio-Quality from Sigma-Aldrich in a 1:1 ratio and stored at -20°C.

3.3 DNA EXTRACTION

The QIAGEN DNA extraction kit was used to extract DNA, following the standard procedure. The kit included all the materials used in this process unless otherwise specified. The principle of the method includes isolating DNA from biological samples using silica-based membrane technology. Initially, 20 µL of protein kinase K was added to a 200 µL sample to lyse the cells. After that, 200 µL of buffer AL was added, and the samples were incubated at 56°C for 10 minutes, followed by 200 µL of ethanol (96%; Antibac). The addition of buffer AL and ethanol helps to bind the DNA from the samples to the column, allowing for the separation of DNA from other components in the sample (Sarnecka et al., 2019).

The next step involved transferring the mixture to a DNeasy Mini spin column in a 2 mL collection tube. The samples were then centrifuged at 8 000 rpm for one minute. After that, the spin column was moved to a new 2 mL collection tube, and 500 µL of Buffer AW1 was added to the column, followed by one minute of centrifugation at 8 000 rpm. Next, 500 µL of Buffer AW2 was added to the column, and the samples were centrifuged for three minutes at 14 000 rpm. Adding buffers AW1 and AW2 helps wash the DNA and remove any impurities or contaminants from the samples, ensuring that only pure DNA is left for further analysis (Sarnecka et al., 2019).

Finally, the column was transferred to a clean 1.5 mL microcentrifuge tube, and 200 µL of Buffer AE was added to elute the sample. The samples were incubated for one minute at room temperature before one minute of centrifugation at 8 000 rpm.

3.3.1 DNA CONCENTRATION ESTIMATION

DNA concentration was estimated using two different methods, Nanodrop and PicoGreen quantification. The values from the Nanodrop quantification were used in further analyses.

3.3.1.1 Nanodrop quantification

DNA samples were quantified using a Nanodrop One UV-Vis spectrophotometer (Thermo Scientific™). This spectrophotometric method measures DNA concentration by determining the absorbance of UV light at 260 nm, which correlates with the amount of DNA present in the sample. Before analysis, the system was calibrated using the same elution buffer AE used during DNA extraction. Two microliters of each sample were loaded onto the spectrophotometer, and their concentrations were measured and documented.

3.3.1.2 PicoGreen quantification

PicoGreen is a fluorescent dye that binds to double-stranded DNA and emits a strong fluorescent signal when bound. Fluorescence is a useful technique that can determine the quantity of DNA by using excitation and emission (Dragan et al., 2010). Compared to absorbance, fluorescence is more sensitive, and can quantify even lower levels of duplex DNA.

A calibration curve was created using a DNA sample with known concentrations to measure the DNA concentrations using PicoGreen. To each well of a black 96-well culture plate (PerkinElmer), 90 µL of MilliQ-H_2O and 0.25 µL of Quant-iT™ PicoGreen (Invitrogen™) were added. Then, 10 µL of DNA sample was added to each well immediately before measuring the fluorescence using excitation and emission wavelengths of 485 and 538 nm with a Fluoroscan plate reader (Thermo Scientific™). The concentrations of DNA in each sample were calculated using the equation from the standard curve made from a DNA sample with known concentrations (**Figure 3.2**).

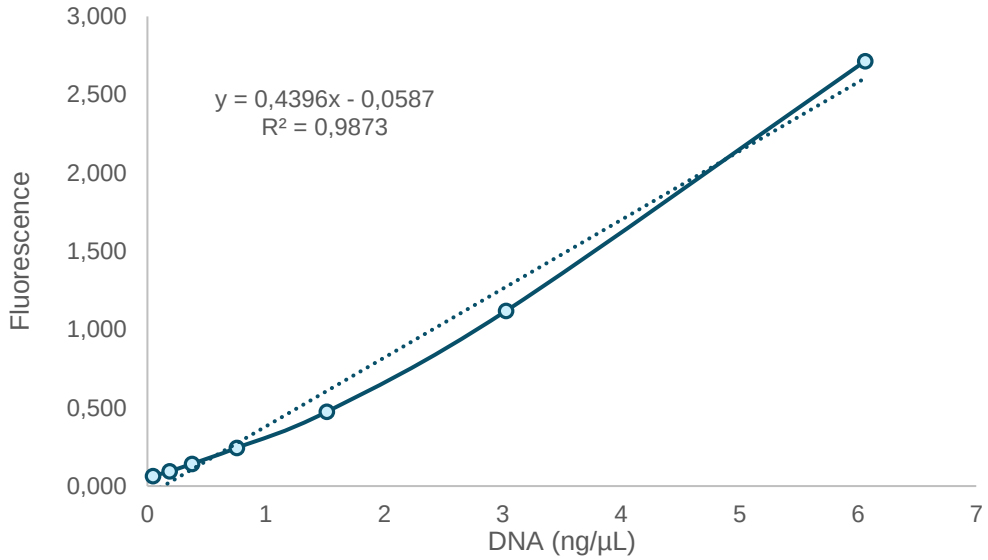

Figure 3.2: Quantification of dsDNA using PicoGreen and a standard curve. *The plot displayed the DNA concentration (ng/µL) of a sample with known concentrations on the x-axis and the corresponding fluorescence measured at an emission wavelength of 538 nm on the y-axis. The equation derived from the trendline was utilized to determine the concentrations of dsDNA.*

3.4 MTDNA DAMAGE ASSAY

The mtDNA damage assay measures DNA damage using quantitative polymerase chain reaction (qPCR). It works by comparing the amplification efficiency of damaged and undamaged templates. This technique is an efficient and cost-effective way of quantitatively analyzing mtDNA with real-time qPCR. It provides high-resolution detection of modifications and is valuable for assessing mtDNA stability, which is crucial for cellular function and genome integrity. Using TaqI restriction enzyme pre-digestion makes it possible to measure mtDNA mutations and nucleic acid alterations reliably. This method has great potential in diverse fields, such as cancer research and age-related disorders (Wang et al., 2015). The principle of the method is shown in **Figure 3.3**.

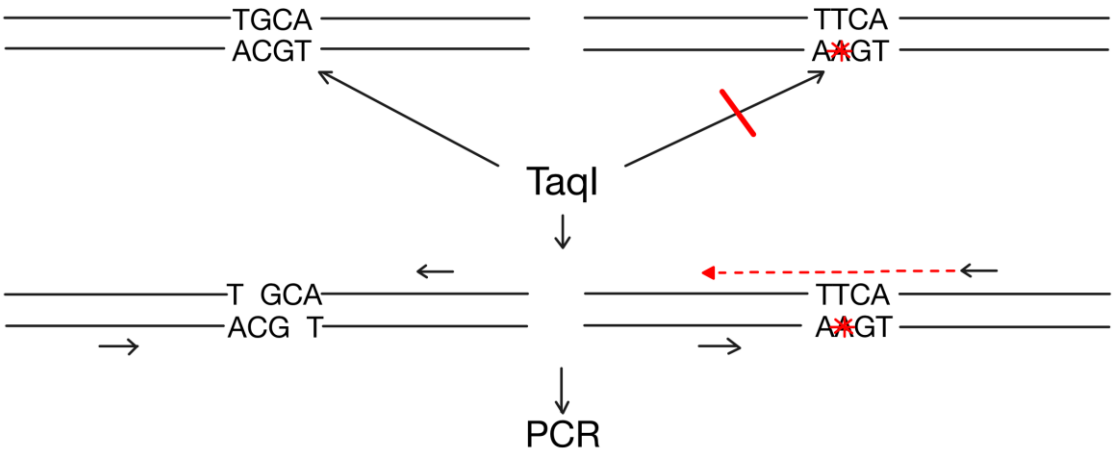

Figure 3.3: Illustration of the principle behind the DNA damage assay. *The qPCR-based DNA damage assay quantifies DNA damage in biological samples by measuring the differential amplification efficiency of damaged vs. undamaged DNA.*

First, a master mix was prepared by mixing Nuclease-Free Water (Ambion), Power SYBR®Green PCR master mix (Applied Biosystems), TaqI, 20 000 U/ml (New England Biolabs), Forward Primer 12S human (Eurofins Genomics), and Reverse Primer 12S human (Eurofins Genomics) according to **Table 3.1**. Primer 12S is a primer for mitochondrial DNA. The instructions for the master mix without TaqI were also used to track nuclear DNA (nDNA), except the primer Ndufa9, an nDNA primer, was used instead of 12S.

Table 3.1: Components used in the qPCR master mix for one reaction, with and without TaqI.

Component	With TaqI - 1 rx (µL)	Without TaqI – 1 rx (µL)
Nuclease-Free Water	0.95	1
SYBR Green (2X)	5	5
TaqI (20U/µl)	0.05	-
Fwd primer (10µM)	0.5	0.5
Rev primer (10µM)	0.5	0.5
Total	7	7

7 µL of the master mix was added to each well of a MicroAmp®Fast 96-well reaction plate (Applied Biosystems). Next, 3 µL DNA, with a concentration of approximately 2 ng/µL, was

transferred to the wells using a multipipette. Each sample was run in triplicates with and without TaqI. The plate was then sealed with MicroAmp^{TM}Optical Adhesive Film (Applied Biosystems). The plate was rotated in a PCR-Plate Spinner (VWR) for approximately one minute to remove any droplets and bubbles. Finally, the analysis was run with a StepOnePlus Real-time PCR system (Applied Biosystems) with the program settings listed in **Table 3.2**.

Table 3.2: Program settings for qPCR analysis of mtDNA damage.

Step	Temperature	Time
1 round	65˚C	15 min
1 round	94˚C	10 min
40 rounds	94˚C	10 s
	60˚C	60 s

3.4.1 MTDNA DAMAGE CALCULATIONS

Outliers were excluded from mtDNA damage calculation if a sample had a Cycle Threshold (C_T) standard deviation (SD) greater than 0.25. The ΔC_T values were obtained by subtracting the C_T mean value of samples without TaqI from the C_T mean value of samples with TaqI. Finally, $2^{(-\Delta C_T)}$ was calculated to normalize the ΔC_T values, transforming them into a linear scale.

3.5 PREPARATION OF OLIGONUCLEOTIDES

Single-stranded oligonucleotides were obtained from Eurofins Genomics, including both fluorescently tagged and un-tagged variants (listed in Appendix C). Complementary pairs of 44-mer oligonucleotides were combined in a 1:1 ratio. This mixture underwent heating to 90°C on a heating block to facilitate oligonucleotide melting, followed by hybridization by cooling to room temperature. The double-stranded oligonucleotides were stored in the freezer at -20°C for future experiments.

3.6 CGAS NUCLEIC ACID BINDING ASSAY

This study used MST to measure the interaction between cGAS and various double-stranded oligonucleotides to determine to which cGAS binds more efficiently. MST measures the

movement of molecules in microscopic temperature gradients, which is sensitive to changes in a molecule's size, charge, and conformation (Jerabek-Willemsen et al., 2011). This enables the quantification of biomolecular interactions by detecting even subtle changes in a molecule when a binding event occurs.

MST was used to measure the interaction between cGAS and three oligonucleotides: complementary DNA, DNA with a mismatch, and an RNA-DNA hybrid (**Figure 3.4**). This project aimed to estimate the binding affinity using the equilibrium dissociation constant K_D. The K_D value refers to the concentration at which half of the protein and oligonucleotides are bound.

Figure 3.4: Illustration of different 44-mer oligonucleotides with a fluorescent tag*. a) complementary DNA, B) complementary DNA with a mismatch at one base pair, and c) RNA-DNA hybrid, where the red strand represents RNA. The fluorescent dye ATTO488 was used to label the DNA strands, while Fluorescein (FAM) was used to color the RNA-DNA hybrid. Both of these dyes emit a green fluorescence upon being excited by light within the blue-to-green range. Figure made in Biorender.com.*

Each combination, cGAS, and oligonucleotide, was analyzed with cGAS and the cGAS-SUMO fusion protein. Initially, 16 tubes were prepared by adding 10 µL of PBS to each. Subsequently, 10 µL of protein was added to the first tube. 10 µL were transferred from the first tube to the second, and this process was continued until the 16th tube. Once the 1:1 dilution series was prepared, 10 µL of fluorescently tagged DNA solution was added to each tube. For the analysis, the samples were transferred to Monolith™ Series Premium Capillaries (NanoTemper), and the examination was carried out using a Monolith NT.115 MicroScale Thermophoresis instrument (NanoTemper) with settings of 100% light emitting diode (LED) power and MST power of 20%, 40%, 80%, and 100%. The analysis was performed with a DNA concentration of 50 nM in each sample and a protein content ranging from 5 800 nM to 0.1770 nM.

3.7 cGAS ENZYMATIC ACTIVITY

The enzymatic activity of cGAS was measured using ELISA to quantify the production of the cGAMP, which is synthesized from cytosolic ATP and GTP under optimized reaction conditions.

3.7.1 ENZYME-LINKED IMMUNOSORBENT ASSAY (ELISA)

cGAS enzymatic activity was determined by quantifying the level of produced cGAMP in enzyme reactions with input nucleic acid (synthetic oligonucleotides or isolated human DNA). cGAMP concentration was determined by ELISA. The commercial kit, 2'3'-cGAMP ELISA Kit (item 501700) from CayMan Chemical, was used for the ELISA assays. Unless otherwise specified, the 96-well plate and all the chemicals, except for recombinant hcGAS, were included in the kit.

3.7.1.1 Preparing enzyme reactions

Enzyme reactions were carried out before initiating the analysis using the ELISA kit. 100 µM of each Transcreener® ATP and GTP (BellBrook Labs), 50 nM cGAS in glycerol, 5 µL buffer E (**Table 3.3**), and the desired amount of DNA sample was mixed. MilliQ-H_2O was added to the samples to make a final volume of 50 µL. The samples were then incubated for 1 hour at 37°C before the addition of Transcreener® Stop & Detect Buffer B (BellBrook Labs) to terminate the reaction.

Table 3.3: Components of buffer E, used in ELISA analysis.

Component	Concentration
Tris pH 7.5	500 mM
NaCl	1.5 M
$MgCl_2$	100 mM
Zinc	2 mM
Tween	0.1%

3.7.1.2 ELISA assay

The production of cGAMP was measured through the ELISA method, in which it competes for a signal. A higher concentration of cGAMP leads to a lower absorbance reading. A series of dilutions was created to make a standard curve with the 2’3’-cGAMP ELISA Standard. 90 µL Immunoassay Buffer C (1X) was added to eight tubes. Next, 10 µL of 2’3’-cGAMP ELISA

Standard was added to the first tube, mixed, and 30 µL transferred to the next tube. This process continued until a dilution series was created.

To prepare a Mouse Anti-Rabbit Immunoglobulin G (IgG)-Coated Plate, the wells were pre-washed with Wash Buffer (1X) five times before adding any reagents. The non-specific binding (NSB) wells and maximum binding (B_0) wells were initially filled respectively with 100 and 50 µL of Immunoassay Buffer C (1X). Then, 50 µL of the 2'3'-cGAMP ELISA Standard dilution series samples were added, followed by 50 µL of the enzyme reaction samples. Next, 50 µL of 2'3'-cGAMP- Horseradish Peroxidase (HRP) Tracer was applied to each of the wells, except for the blank (Blk) and total activity (TA) samples. Within 15 minutes, 50 µL of 2'3'-cGAMP ELISA Polyclonal Antiserum was added to all the wells except for the TA, NSB, and Blk wells. The plate was then covered with a 96-Well Cover Sheet and refrigerated at 4°C overnight.

The wells were emptied and washed with Wash Buffer (1X) five times before developing the plate. 175 µL of 3,3´,5,5´-tetramethylbenzidine (TMB) Substrate Solution was added to all the wells, and 5 µL of Tracer was added to the TA wells. The plate was covered and incubated at room temperature for 30 minutes before adding 75 µL of HRP Stop Solution to all the wells and reading the plate at 450 nm.

3.7.1.3 Standard curve

The ELISA standard serial dilution samples' absorbance was measured. To begin with, the Corrected B_0 was calculated by subtracting the NSB absorbance from the B_0 absorbance. After that, the standard bound/maximum bound (B/B_0) was calculated using **Equation 1**:

$$\frac{B}{B_0} = \frac{X - NSB}{Corrected\ B_0} \quad (1)$$

B/B_0 is the standard bound/maximum bound ratio. X is the absorbance measured for the sample, NSB refers to the absorbance measured for the NSB wells.

The final calculation before creating the standard curve was a logit transformation performed to linearize the data using **Equation 2**:

$$logit\left(\frac{B}{B_0}\right) = \ln\left[\frac{\frac{B}{B_0}}{1-\frac{B}{B_0}}\right] \quad (2)$$

Figure 3.5 illustrates an example of a standard curve from this project and the equation obtained from the linear regression of the standard curve data.

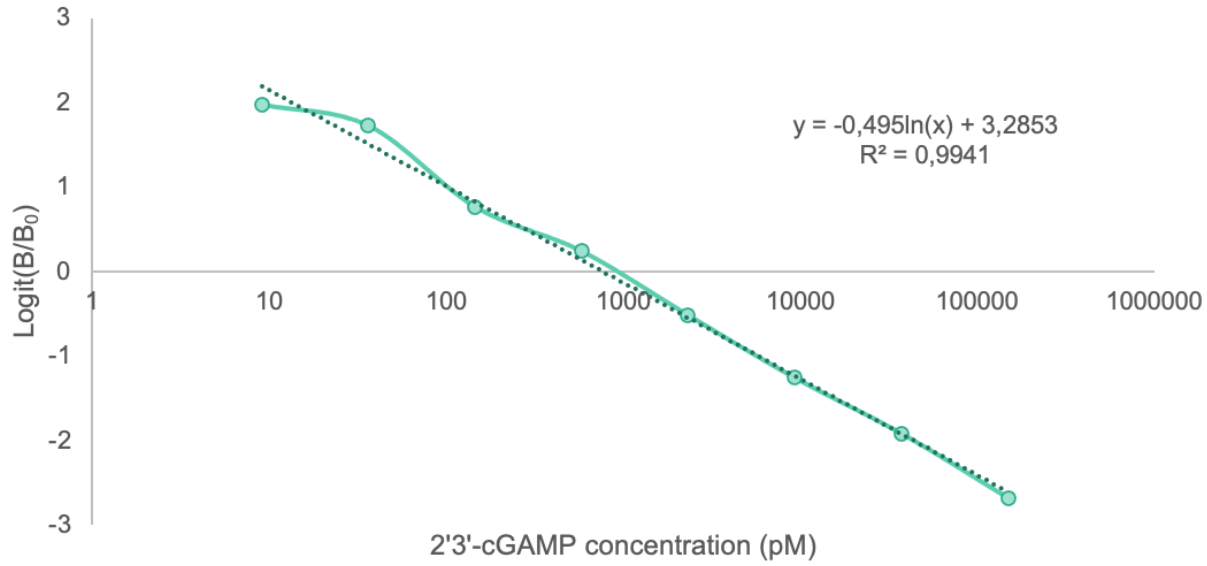

Figure 3.5: Standard curve obtained from a dilution series of 2'3'-cGAMP ELISA standard. *The y-axis shows the linearized version of the standard bound divided by the maximum bound. The logarithmic x-axis shows the concentration of 2'3'-cGAMP in the samples, measured in picomolar. The standard curve plot equation in the top right corner is used to calculate the 2'3'-cGAMP concentrations in the samples with unknown concentrations. The R^2 value, the coefficient of regression, is also shown in the top right corner.*

3.7.1.4 Calculations of 2'3'-cGAMP concentration

To determine the concentration of 2'3'-cGAMP produced in the enzyme reactions with the patient samples, the B/B_0 and $\ln(B/B_0)$ were calculated similarly to the standard samples. Finally, the linearized B/B_0 value and the values from the equation of the standard curve (**Equation 3**) were utilized to estimate the concentration of cGAMP**.**

$$x = EXP(\frac{y-b}{a}). \quad (3)$$

x is the calculated cGAMP concentration, EXP is the inverse of the natural logarithm function (ln), y is the calculated logit (B/B_0) values (from **Equation 2**), *b* is the y-intercept of the standard curve, and *a* is the slope of the standard curve.

3.7.1.5 Analysis performed with ELISA

Based on optimization, 60 ng of isolated EV-DNA was decided in general to use as DNA concentration in the hcGAS enzymatic reaction. For samples that were treated with RNase, 17 µL of sample was mixed with 2 µL of 10xNEBuffer 3 (BioLabs), and the samples were then split into two. One aliquot was added 1 µL RNase If (BioLabs), and the other was added 1 µL MilliQ-H_2O. The ELISA assay was then performed with the same amount of cGAS, but the amount of DNA was reduced to 30 ng due to a shortage of patient material and low DNA concentrations in the patient samples. These factors would make it challenging to compare the samples if higher levels of DNA were to be used, as not all the sample could be analyzed with the same amount of DNA in the final samples for the assay.

In this project's last cGAMP production assay, the cGAMP levels were determined by conducting enzyme reactions with 50 nM of various oligonucleotides. The oligonucleotides used in the assay were double-stranded complementary DNA, DNA-RNA hybrid, DNA-uDNA, apDNA, mismatch DNA (mmDNA), ssDNA, and ssRNA. uDNA is a molecule where the usual thymine (T) bases are replaced by uracil (U), typically found in RNA. apDNA is an abbreviation for apurinic/apyrimidinic DNA (Cadet & Wagner, 2013). This term describes DNA that has experienced damage resulting in the loss of a purine or pyrimidine base. Exposure to genotoxic agents, ionizing radiation, or reactive oxygen species can lead to such DNA damage. A statistical analysis was employed to compare the oligonucleotides to the DNA duplex and assess any significant differences between the two. Specifically, a student's t-test was conducted, and the resulting p-values were used to determine the statistical significance of the comparison, with $p<0.05$.

4 RESULTS

4.1 PROTEIN PURIFICATION

The cGAS was expressed as a 6xHistag-SUMO-cGAS fusion protein (**Figure 4.1**) and affinity purified using IMAC, followed by SEC, which purified the protein based on size. The size of recombinant cGAS and purity levels were confirmed through SDS-PAGE analysis.

***Figure 4.1: cGAS-SUMO fusion protein illustration**. The orange box demonstrates the 6xHis-tag; blue shows the SUMO protein; red is the TEV protease cleavage site, and green shows the cGAS protein.*

4.1.1 AFFINITY CHROMATOGRAPHY PURIFICATION OF CGAS

E.coli was transformed with an expression plasmid for recombinant fusion 6xHistag-SUMO-cGAS. The cGAS protein was induced by IPTG at 18°C overnight. As described in the methods, cGAS was purified from cell-free lysate by IMAC. To confirm the presence of the SUMO-cGAS fusion protein, SDS-PAGE was performed using the SeeBlue Standard as a reference ladder. The most protein-rich fractions were pooled for further purification. A representative gel from one of the purification rounds is shown in **Figure 4.2**, with the first lane displaying the SeeBlue ladder, followed by the flowthrough and washing steps. The subsequent three lanes show the elution with buffer B (50mM imidazole), and the last three lanes show the elution with buffer C (300mM imidazole). The 6xHistag-SUMO-cGAS fusion protein, with a molecular mass of 57 kDa, is indicated by the band between 51 and 64 kDa. The thicker band found between 14 and 19 kDa is presumably SUMO, as SUMO has a molecular weight of approximately 11 kDa (Park-Sarge & Sarge, 2009). However, when added to SDS-PAGE, the size usually increases to 15-17 kDa. Although the SDS-PAGE confirms the presence and relative abundance of expressed cGAS, additional purification steps were performed to ensure low contaminating activity in later assays.

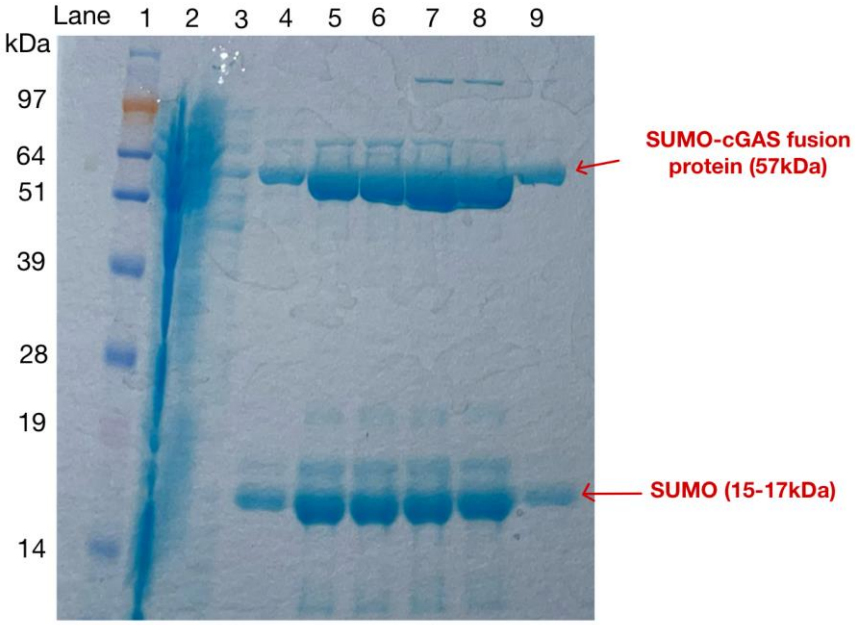

Figure 4.2: SDS-PAGE gel showing fractions after IMAC purification. *Lane 1 is the SeeBlue Standard, while lanes 2-3 show the flowthrough and wash fractions. Lanes 4-6 and 7-9 were loaded with samples taken from elution fractions with buffer B (50mM imidazole) and C (300mM imidazole), respectively. The samples were loaded onto a 12% Bis-Tris plus 10-well gel.*

4.1.2 SIZE EXCLUSION CHROMATOGRAPHY PURIFICATION OF CGAS

SEC was used for the next purification step. For the purification of protein based on size, porous particles in an Enrich SEC 70 column were used as the stationary phase while PBS was used as the mobile phase. A chromatogram displaying the elution of protein in a purification round conducted by SEC is shown in **Figure 4.3**.

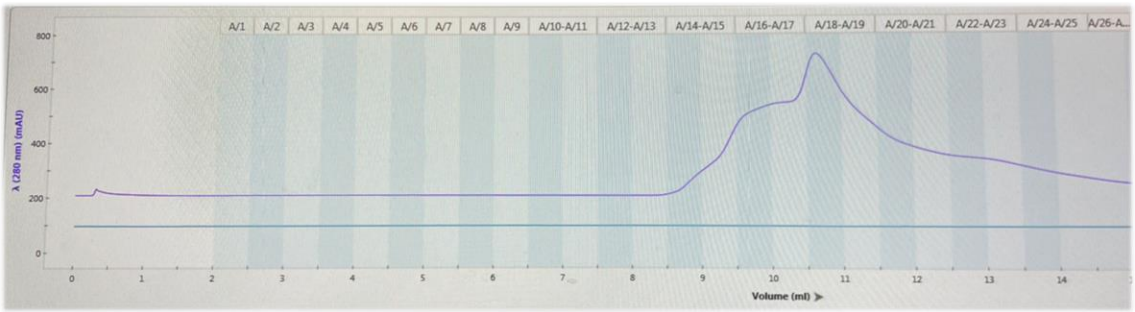

Figure 4.3: SEC chromatogram of cGAS-SUMO fusion protein. *The volume (mL) of PBS used during protein elution is represented on the X-axis, while the absorbance measured at 280 nm in milli-absorbance units is presented on the Y-axis. The protein was eluted in fractions of 500 µL, and the fractions that showed a peak in absorbance at 280 nm were analyzed using SDS-PAGE.*

The peak that appeared in the chromatogram indicated the fractions with the highest protein concentrations. These fractions were then subjected to further analysis by SDS-PAGE to assess the purity, as shown in **Figure 4.4**. The gel indicates that the cGAS protein (57 kDa) was present in all selected fractions, with the most significant amount in lanes 3-6. Lanes 5-8 show a significant band between 14 and 19 kDa, which might correspond to free SUMO (15-17 kDa).

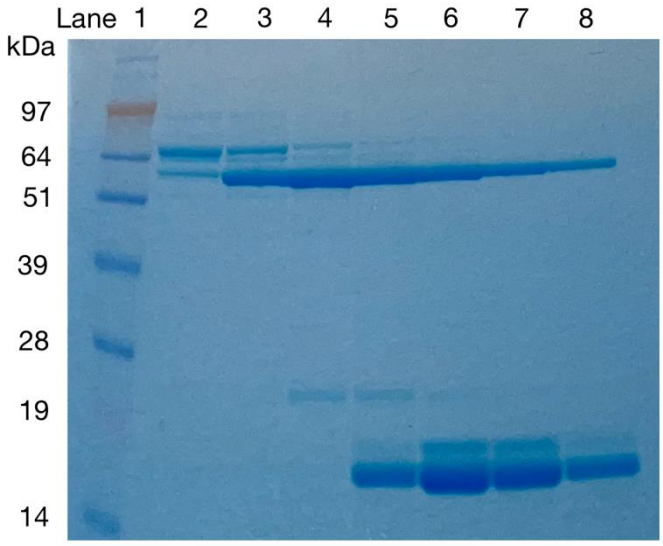

Figure 4.4: Gel of fractions rich in protein after purification with size exclusion chromatography. *Lane 1 contains the SeeBlue Standard, while lanes 2-8 include fractions that were eluted with SEC. The samples were loaded onto a 12% Bis-Tris plus 10-well gel.*

4.1.3 SUMO-TAG REMOVAL

The fusion protein 6xHistag-SUMO-cGAS has a TEV protease cleavage site between the SUMO and cGAS sites. TEV protease was therefore added to the protein to remove the SUMO tag from the fusion protein. Ni^{2+}-NTA agarose was used to remove the released 6xhis-tagged SUMO fragment. The molecular masses of the 6xHistag-SUMO-cGAS fusion protein, cGAS, and free SUMO are approximately 57kDa, 43kDa, and 15-17kDa, respectively. **Figure 4.5A** illustrates a sample before (lane 3) and after (lane 2) the addition of TEV protease, and **Figure 4.5B** shows the sample after the addition of TEV protease, before (lane 3) and after (lane 2) Ni^{2+}-NTA agarose cleanup.

Ni^{2+}-NTA agarose was used to remove the released 6xHis-tagged SUMO fragment. The molecular masses of the 6xHistag-SUMO-cGAS fusion protein, cGAS, and free SUMO are approximately 57kDa, 43kDa, and 15-17kDa, respectively.

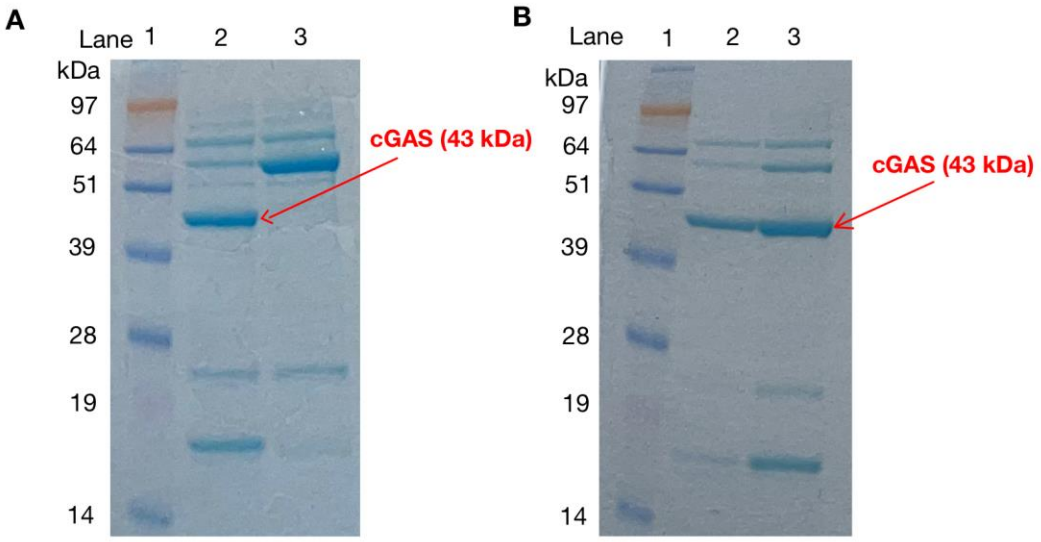

Figure 4.5: SDS-PAGE gel after cleavage of SUMO-tag with TEV protease. *The gel used for the SUMO-tag removal via SDS-PAGE was a 12% Bis-Tris gel with 10 wells. Lane 1 was reserved for the SeeBlue Standard ladder. On gel* ***A****, lane 2 show the TEV protease-treated sample, while lane 3 contained the untreated cGAS-SUMO fusion protein sample. On gel* ***B****, lane 2 showed the cleaned-up, cleaved cGAS-SUMO, which had been treated with* Nickel NTA agarose. *Lane 3 contained the cleaved but uncleaned sample.*

4.2 Exploring the DNA binding and cGAMP synthesis activities of cGAS

This project focuses on the protein cGAS, specifically investigating its binding affinity and ability to induce production of cGAMP. The aim is to examine the capacity of cGAS to stimulate cGAMP production when exposed to DNA from synthetic or human origins. DNA binding was explored by three defined, synthetic oligonucleotides.

4.3 cGAS nucleic acid binding assay

During MST, the motion of fluorescent molecules (oligonucleotides) is monitored upon a generated temperature gradient. When the oligonucleotide and cGAS are bound together, their movement as a complex differs from when they are unbound, which can be detected by MST. Three different types of oligonucleotides were tested: DNA duplex, DNA mismatch, and RNA-DNA hybrid. The assay was performed on both the cGAS protein and the 6xHistag-SUMO-cGAS fusion protein. **Figure 4.6** shows the dose-response of the analyses with cGAS. The results from the fusion protein were very similar and can be found in Appendix D. The RNA-

DNA hybrid (**Figure 4.6C**) was the only oligonucleotide with a clear sigmoidal dose-response curve (presented in **Figure D.2** in appendix D), indicating a binding affinity approximately 10 times greater than the DNA duplex and mismatch (**Figure 4.8A and 4.8B**). The RNA-DNA hybrid showed a K_D value of approximately 0.8 µM ± 0.1 µM, where 50% of the protein is bound to the DNA (see **Figure D.3** in Appendix D). The values for the two other oligonucleotides could only be roughly estimated based on the curves in **Figure 4.6A and 4.6B** (**Table 4.1**). The results indicate that the RNA-DNA hybrid exhibits a significantly higher binding affinity to cGAS than the DNA duplex and DNA mismatch.

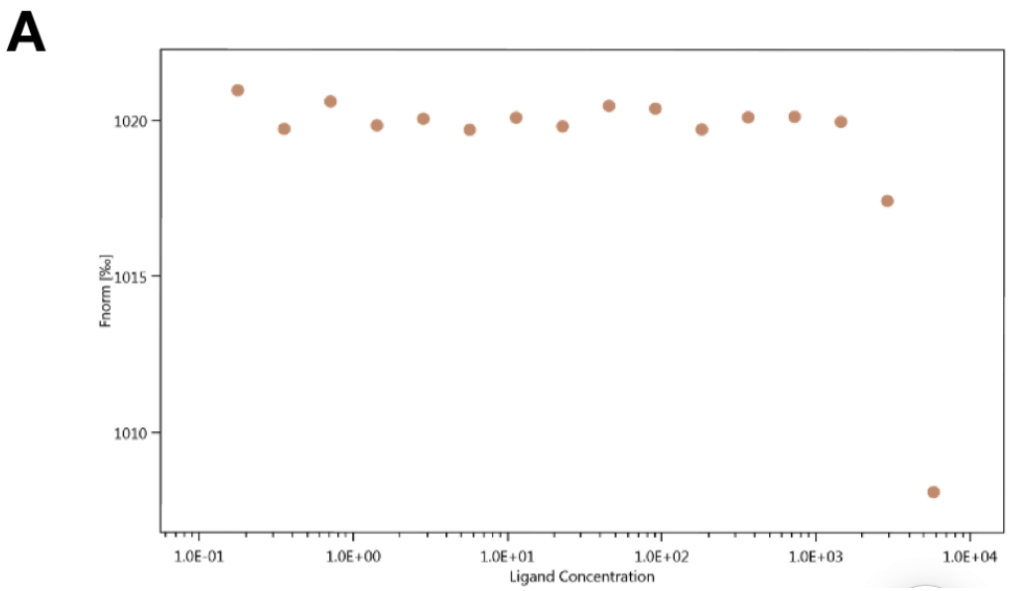

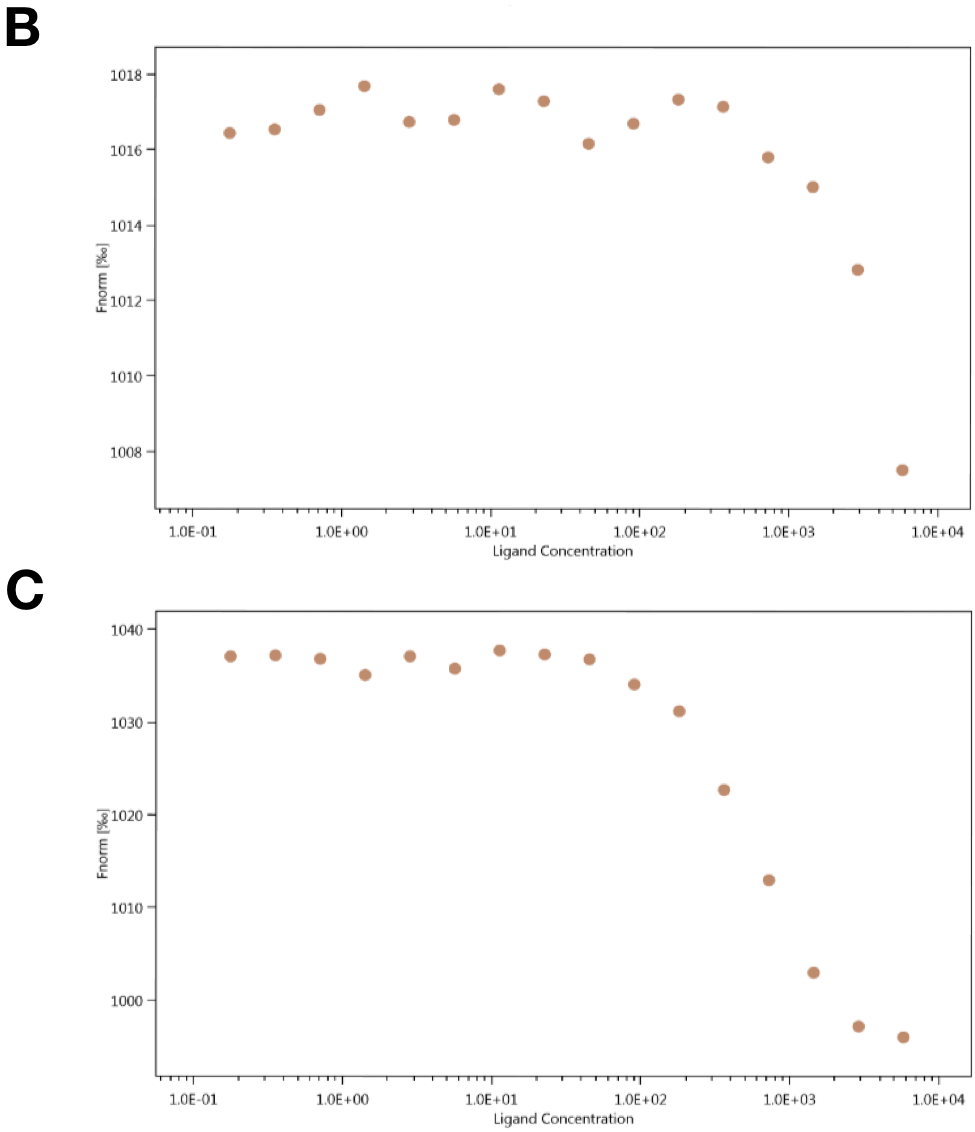

Figure 4.6: Dose response from analyzing binding affinity with Microscale Thermophoresis. *The graphs display the normalized change of fluorescence (‰) plotted against the ligand concentration (nM) for three different scenarios:* ***A)*** *DNA duplex,* ***B)*** *DNA with a mismatch, and* ***C)*** *RNA-DNA hybrid.*

Table 4.1: K_D50 values for binding of cGAS to the different oligonucleotides. *The values for the DNA duplex and DNA mismatch are estimated values.*

Oligonucleotides	K_D (µM)
DNA duplex	>7.5
DNA mismatch	>7.5
RNA-DNA hybrid	~0.8 ± 0.1

4.4 cGAS ENZYMATIC ACTIVITY

The enzymatic activity of cGAS was measured by cGAMP production quantified using an ELISA assay. To ensure its functionality, the recombinant cGAS was tested and compared to a commercial cGAS with dsDNA of 44 bp as the activating factor. The results, shown in **Figure 4.7**, confirmed that the recombinant and commercial cGAS were approximately equally efficient. However, the recombinant protein shows less variation between duplicates. Optimization was carried out before analyzing the human material to ensure a successful analysis.

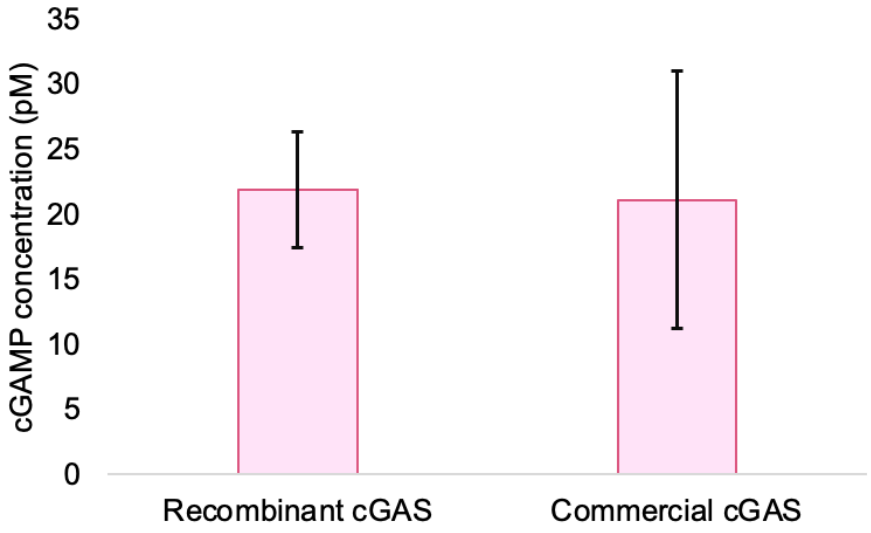

Figure 4.7: Confirming enzymatic activity of recombinant cGAS. *The bars display the results of cGAMP quantification using ELISA with both recombinant and commercial cGAS. The error bars represent the standard deviation. The cGAMP concentration is presented as the mean value from two parallels.*

4.4.1 OPTIMIZATION

Before analyzing the human material with ELISA assay, the buffer conditions were optimized, and the appropriate cGAS variant from the purification steps was selected. DNA titration was performed to determine the suitable amount of isolated DNA from human samples. The initial cGAS enzymatic reaction was carried out using Buffer D [5 mM $MgCl_2$, 0.01% Brij-35, 1% DMSO], which resulted in minimal cGAMP quantities. Subsequently, the assay was conducted using Buffer E [50 mM Tris pH 7.5, 150 mM NaCl, 10 mM $MgCl_2$, 200 µM $ZnCl_2$, 0.01% Tween], leading to a significant change in absorbance, demonstrating the essential role of zinc in cGAS activity. A titration curve was then made with concentrations of 0.1, 1, 10 and 100 nM of cGAS and 30 nM of DNA (commercial Interferon-Stimulatory DNA (ISD); BellBrook

Labs), confirming that Buffer E was suitable for this enzyme reaction. **Figure 4.8** illustrates the titration curve, where a higher concentration of cGAS results in a higher cGAMP concentration detected at an absorbance of 450 nm. This indicates that a higher concentration of cGAS in the enzyme reaction results in an increased cGAMP production.

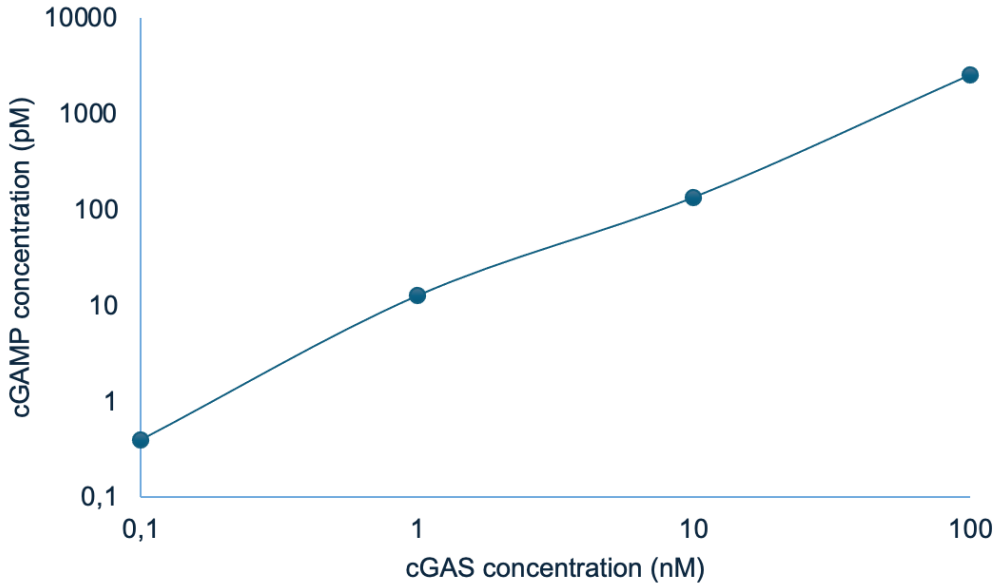

Figure 4.8: Titration curve confirming enzymatic reaction using Buffer E. *The x-axis represents the cGAS concentration in nM, and the y-axis represents the detected cGAMP concentration calculated using a standard curve (see figure 3.5 in materials and methods). The DNA used for this optimization step is commercially bought DNA at a length of 45 base pairs.*

To determine the optimal cGAS variant, cGAMP production was evaluated using 30 nM of each; cGAS and commercial DNA. **Figure 4.9** presents the production of cGAMP for the various variants. The cGAS variants showed similar levels of cGAMP production, indicating comparable enzymatic activity under the tested conditions; however, the fusion protein stored in glycerol exhibited slightly higher levels of cGAMP. Given that this protein was stored in glycerol in the freezer, its quality would likely degrade at a slower rate, allowing for the possibility of using the same protein to analyze all patient samples. include truncated protein stored on ice (TP-ice), fusion protein stored on ice (FP-ice), truncated protein mixed with glycerol in a 1:1 ratio and stored in the freezer at -20°C (TP-G), and fusion protein mixed with glycerol in a 1:1 ratio and stored in the freezer at -20°C (FP-G).

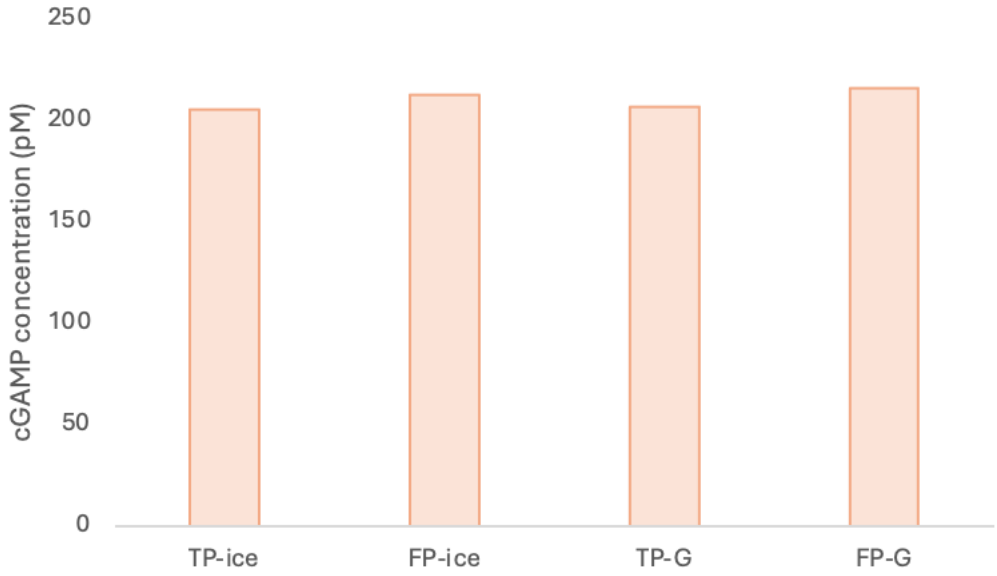

Figure 4.9: Selection of cGAS variant for further studies. *The x-axis displays different cGAS variants, including fusion (FP) and truncated (TP) proteins, under different conditions - fresh on ice or mixed with glycerol and stored in the freezer at -20°C. The y-axis represents cGAMP production in pM measured with ELISA.*

A titration curve (**Figure 4.10**) was conducted to determine the optimal DNA amount from human samples. DNA from EVs was used in amounts of 0, 20, 40, 60, and 80 ng. The most responsive range was found between 40 to 60 ng of EV-DNA. An amount of 60 ng was therefore selected to analyze the patient samples.

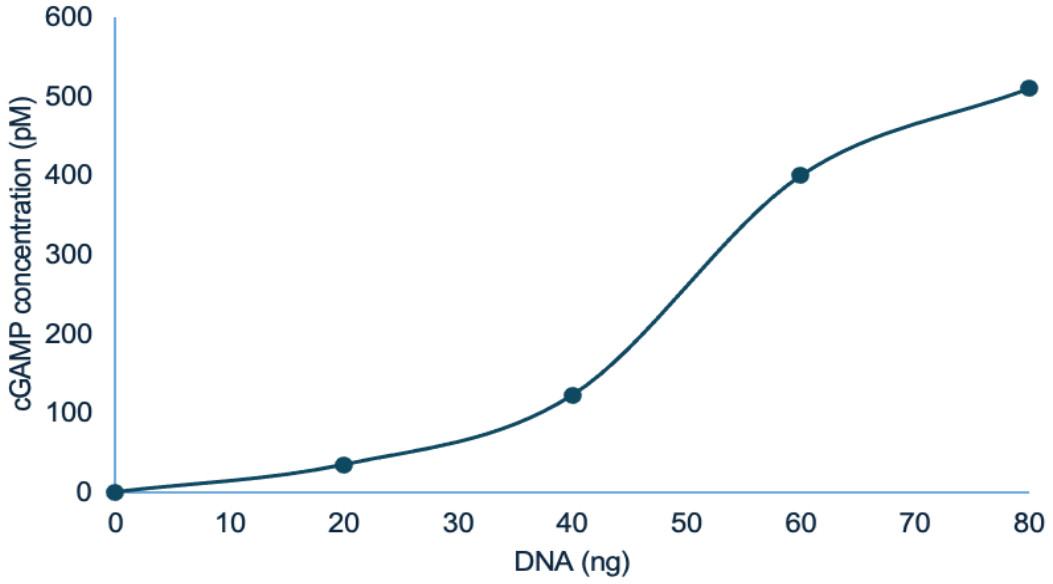

Figure 4.10: cGAS activation as a function of increasing EV DNA. *The x-axis represents the amount of EV DNA used in the analysis, and the y-axis shows the cGAMP levels detected through ELISA.*

4.4.2 ENZYMATIC ACTIVITY USING VARIOUS OLIGONUCLEOTIDES

ELISA was conducted on various oligonucleotides to investigate differences in enzymatic activity. The enzymatic reactions contained 50 nM of cGAS and oligonucleotides, and both single-stranded and double-stranded DNA and RNA were examined. **Figure 4.11** shows the detection of cGAMP using the various oligonucleotides. The results showed minimal variation, with approximately 20 pM being the most significant difference. Among the tested substrates, the DNA duplex, DNA:U-DNA, and DNA mismatch demonstrated the highest levels of cGAMP production, indicating their tendency to trigger cGAS-STING pathway activation. Conversely, the RNA-DNA hybrid, apDNA, and ssDNA exhibited lower levels of cGAMP production. Notably, ssRNA fell between these values, indicating a moderate ability to induce cGAMP production. Student's t-test comparing the different oligonucleotides to the DNA (DNA:DNA) duplex resulted in p-values higher than 0,05 in all cases, indicating no significant difference between the oligonucleotides. For the RNA-DNA hybrid, DNA:U-DNA, apDNA, mmDNA, ssDNA and ssRNA, the p-values were 0.16, 0.72, 0.20, 0.95, 0.12 and 0.52, respectively.

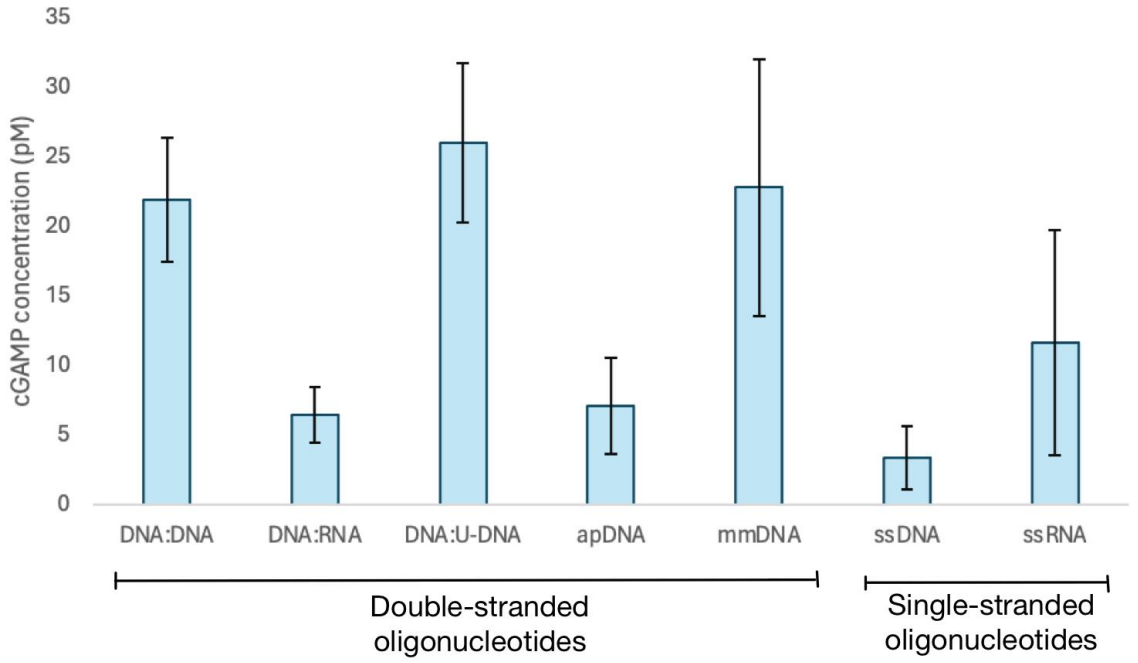

Figure 4.11: cGAS enzymatic activity measured with different oligonucleotides. *The x-axis shows the different oligonucleotides used, while the y-axis indicates the detected produced cGAMP by cGAS. The first five poles (DNA: DNA - mmDNA) are double-stranded oligonucleotides, and the last two are single-stranded DNA and RNA. The standard deviation is shown by the error bars.*

4.4.3 PATIENT MATERIAL: INVESTIGATING THE IMPACT OF CIRCULATORY FACTORS ON CGAS ACTIVATION

The study investigated two types of samples, EVs, and plasma, from patients with sepsis or organ failure without sepsis. The EV samples from controls were different from plasma controls. The plasma control group consisted of controls from three groups: fasted, non-fasted, and individuals with rare metabolic disorders. DNA was isolated from pre-isolated EV from patients with sepsis and organ failure, and healthy controls, as well as from plasma from the same patient groups. The concentration of isolated DNA from human samples were analyzed using Nanodrop and PicoGreen to quantify nucleic acids, and qPCR was used to detect mtDNA and nDNA.

It was found that the concentrations of nucleic acids were too low to yield any PicoGreen intensities (Appendix F, **Figure F.1)**. On the other hand, the Nanodrop analysis indicated the presence of nucleic acids. However, it is essential to note that this method measures the light absorbed by bases in nucleic acids as well as in free nucleotides. Therefore, it can be difficult to accurately control for the amount of nucleic acids that activate cGAS based exclusively on the amount from Nanodrop analyses.

The C_T values (from the qPCR analyses) is a separate method that can be used to specifically quantify the amount of mtDNA and nDNA (fragments) in the samples, adjusted for input DNA determined by Nanodrop analyses. **Figure 4.12** shows the relative amount of mtDNA present in the EV samples and **Figure 4.13 and 4.14** presents the amount of mtDNA and nDNA in the plasma samples, respectively.

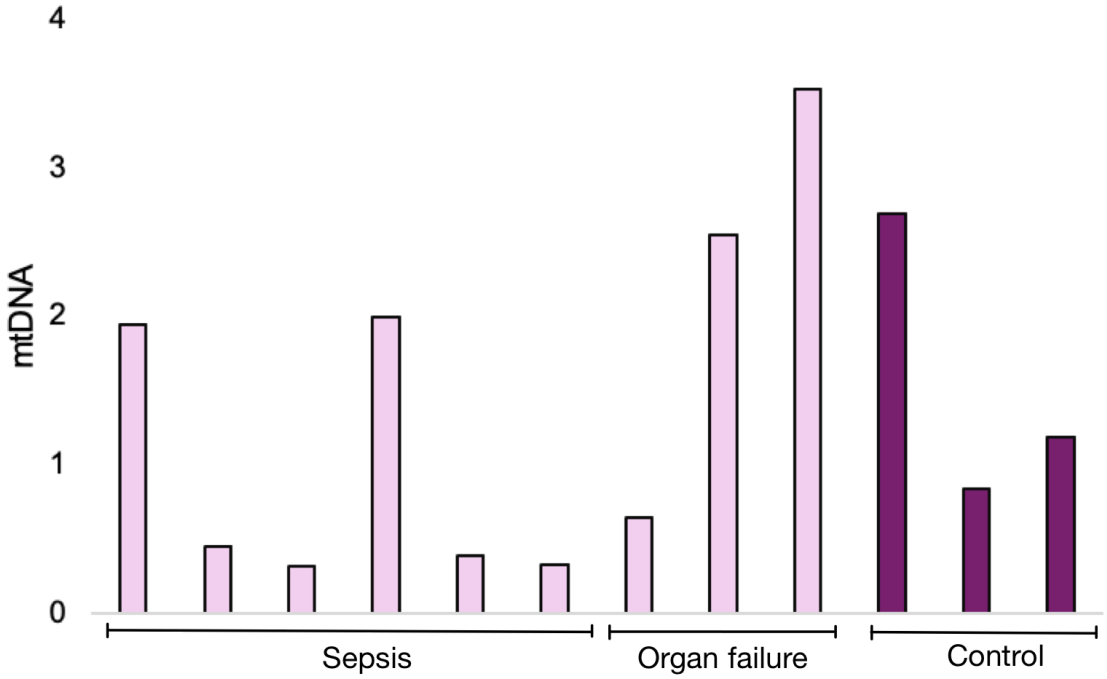

Figure 4.12: the amount of mtDNA present in EVs of sepsis and non-sepsis patients. *Light purple represents relative amount of mtDNA in EVs of sepsis and organ failure patients, while dark purple represents EVs of non-sepsis patients. The x-axis shows different samples, and the y-axis shows relative amount of mtDNA determined by qPCR calculated as* $2^{Average\ C_T - C_T}$.

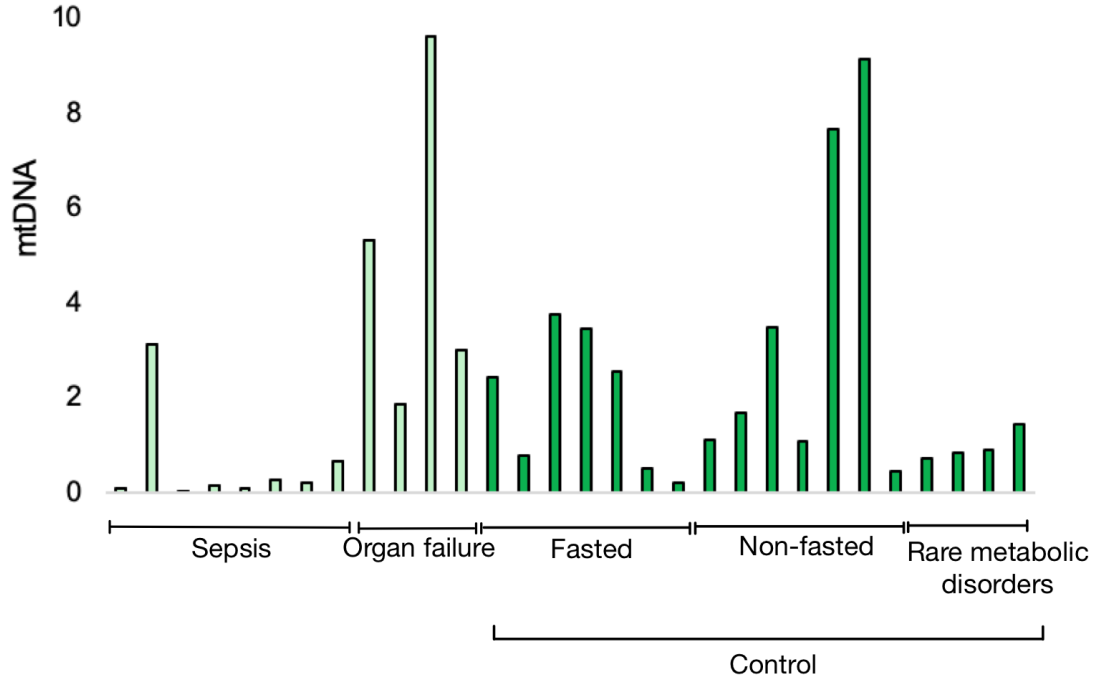

Figure 4.13: the amount of mtDNA present in plasma samples of sepsis and non-sepsis patients. *Light green represents relative amount of mtDNA in plasma samples of sepsis and organ failure patients, while dark green represents plasma samples of non-sepsis patients. The x-axis shows different samples, and the y-axis shows relative amount of mtDNA determined by qPCR calculated as* $2^{Average\ C_T - C_T}$.

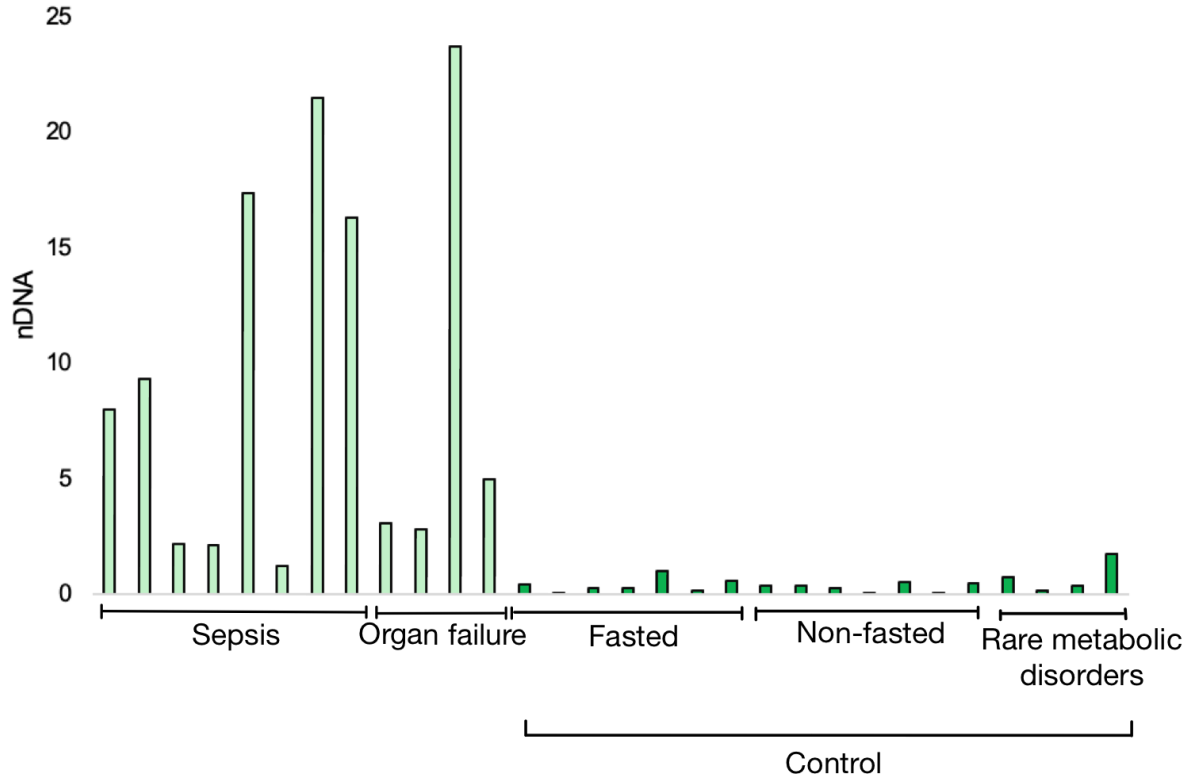

Figure 4.14: The amount of nDNA present in plasma samples of sepsis and non-sepsis patients. *Light green represents relative amount of nDNA in plasma samples of sepsis and organ failure patients, while dark green represents plasma samples of non-sepsis patients. The x-axis shows different samples, and the y-axis shows relative amount of nDNA determined by qPCR calculated as* $2^{Average\ C_T - C_T}$.

Figure 4.15 shows the correlation between the Nanodrop and C_T values, converted to an estimated copy number, of mtDNA in both EV (blue) and plasma (purple) samples, and **Figure 4.16** illustrates the nDNA estimated copy number of the plasma samples. The EV samples had levels of nDNA that were too low to be detected using qPCR. The analysis revealed no significant correlation between mtDNA and nDNA levels, and DNA concentrations determined by Nanodrop analyses.

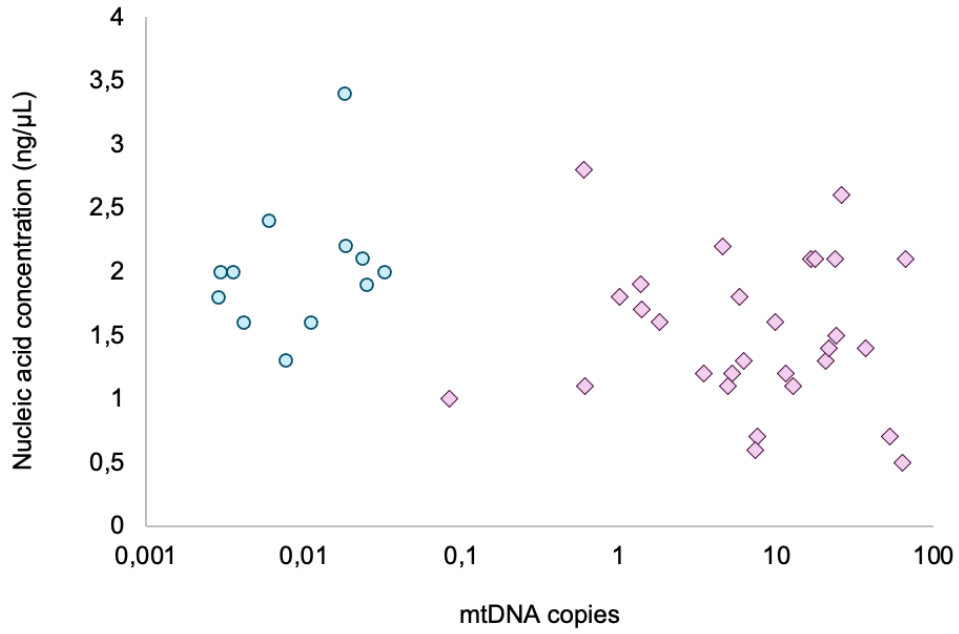

Figure 4.15: Investigation of the relationship between the presence of mtDNA copies and nucleic acid concentration. *The x-axis shows the relative amount of mtDNA. The y-axis shows the nucleic acid concentration measured in ng/µL, quantified using Nanodrop. The purple squares illustrate plasma samples, and the blue circles are EV samples.*

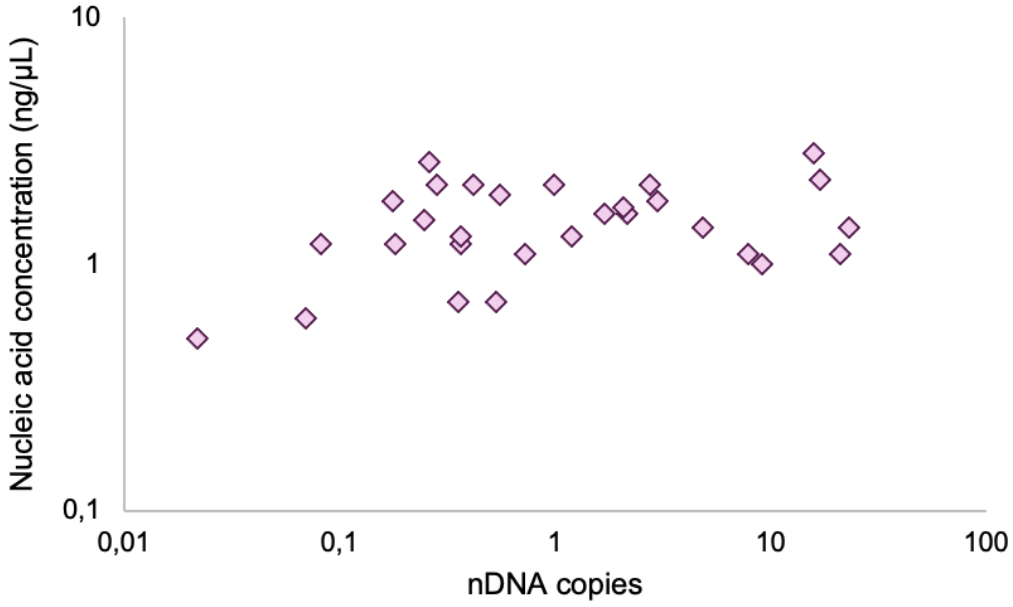

Figure 4.16: Investigation of the relationship between the presence of nDNA and nucleic acid concentration. *The x-axis shows the relative amount of nDNA. The y-axis shows the nucleic acid concentration measured in ng/µL, quantified using Nanodrop. The purple squares illustrate plasma samples.*

4.4.4 Quality of DNA in circulation: free versus EV-embedded, mtDNA and nDNA

The samples were analyzed for mtDNA damage using a qPCR-based method combined with TaqI digestion. All samples were analyzed in triplicates, allowing for the exclusion of outliers where the CT standard deviation was higher than 0.25. **Figure 4.17** and **Figure 4.18** show the estimated mtDNA damage in the EV and plasma samples, respectively. The controls are shown in a dark color. The EV samples contained mtDNA that was more damaged than in the plasma samples. No clear difference within the three groups, was observed. Yet, when looking at the plasma samples, mtDNA in the sepsis and organ failure groups appear slightly less damaged than the control.

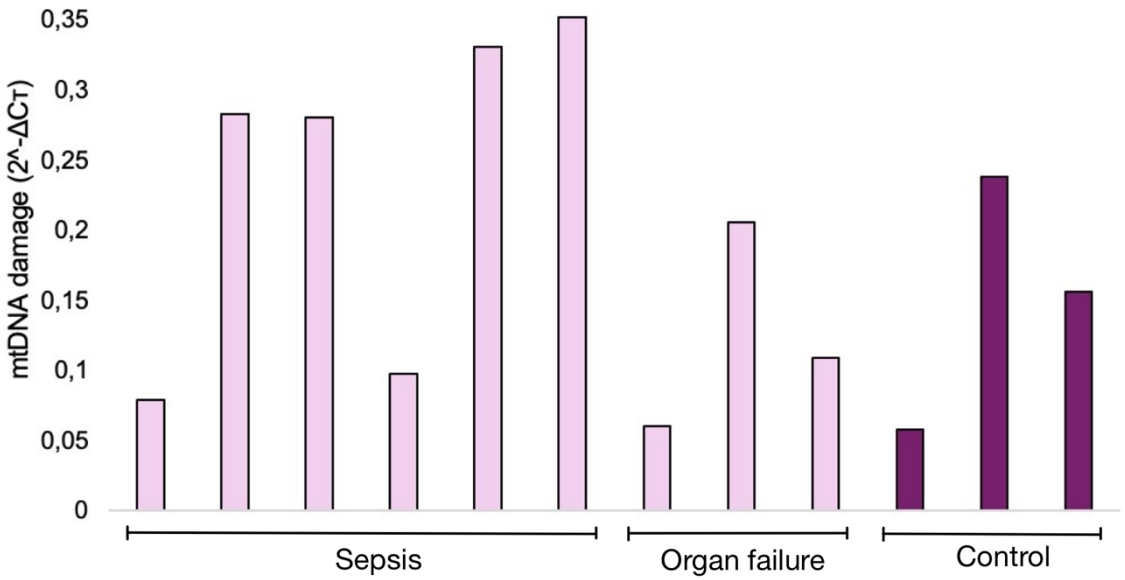

Figure 4.17: mtDNA damage in EVs of sepsis and non-sepsis patients. *Light purple represents mtDNA damage in EVs of sepsis and organ failure patients, while dark purple represents EVs of non-sepsis patients. The x-axis shows different samples, and the y-axis shows mtDNA damage calculated as* $2^{-\Delta CT}$.

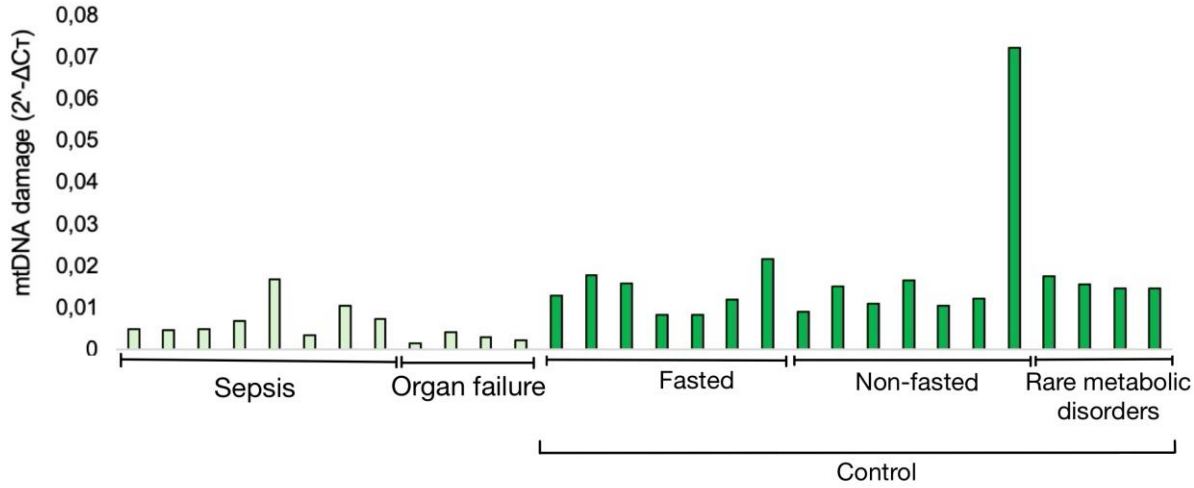

Figure 4.18: mtDNA damage in plasma samples of sepsis and non-sepsis patients. *Light green represents mtDNA damage in plasma samples from sepsis and organ failure patients, while dark green indicates samples from control patients (fasted, non-fasted and rare metabolic disorders). The x-axis shows different samples, and the y-axis shows mtDNA damage calculated as* $2^{-\Delta CT}$.

4.4.5 Activation of cGAS by isolated DNA from human samples

cGAS was activated with defined amounts of isolated human DNA from the different groups. Activation was measured as cGAMP and detected by ELISA. As shown in **Figure 4.19**, the assay conducted on the human patient samples did not show apparent differences between the patient groups. Since the Nanodrop analyses do not correlate with the qPCR-based quantification of mtDNA (**Figure 4.15**), the results were normalized to the number of mtDNA (found in **Figure 4.12**) and presented in **Figure 4.19B and 4.20B** for EVs and plasma samples, respectively. The results indicated stronger activation of cGAS when using mtDNA-containing isolated DNA from sepsis patients. DNA isolated from plasma (**Figure 4.20A**) induced a higher production of cGAMP by cGAS in all three groups compared with the EV samples. Similarly, as for EV-DNA (**Figure 4.19**), cGAMP production using DNA from plasma was also normalized to mtDNA copies. Here, plasma DNA from sepsis patients was as efficient as DNA from controls in activating cGAS. A figure comparing the EV and plasma samples with each other is found in Appendix E.

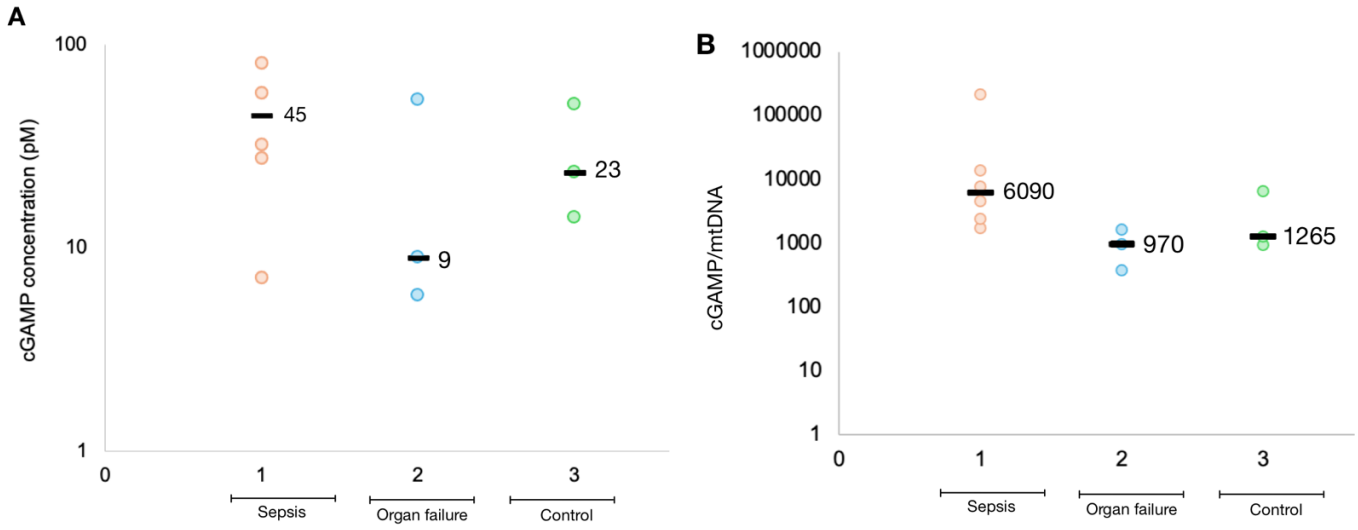

Figure 4.19: cGAS activation using 60 ng DNA isolated from EVs. *The x-axis represents different patient groups: 1 (orange) for sepsis patients, 2 (blue) for patients with organ failure, and 3 (green) for control patients. The y-axis in panel (A) shows the detected cGAMP concentration analyzed with ELISA and panel (B) shows the quantified cGAMP per mtDNA. The black lines on the graphs and their respective numbers represent the median value.*

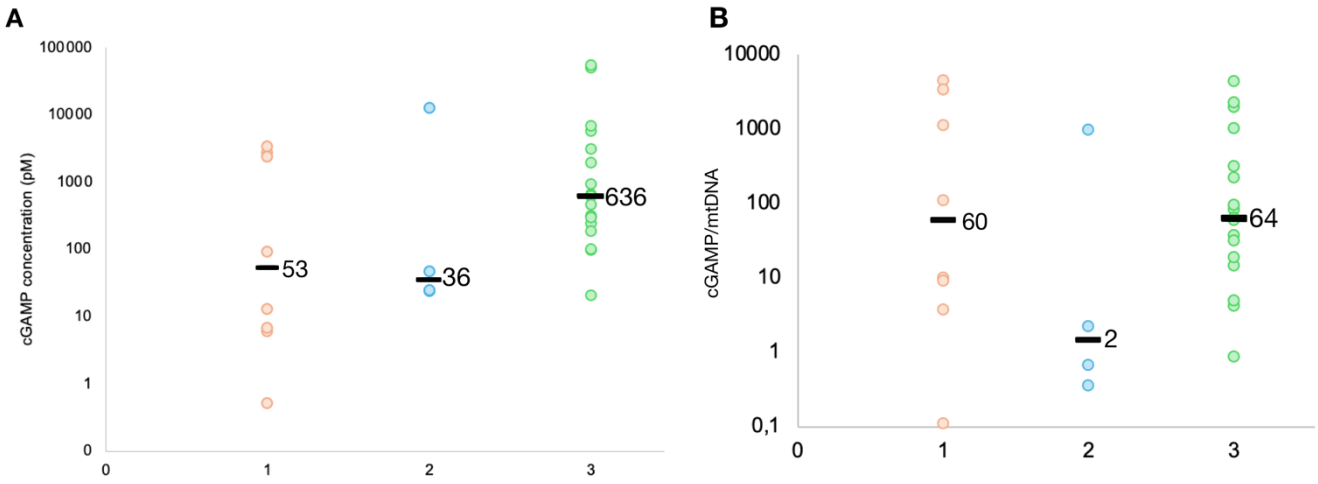

Figure 4.20: cGAMP Detection using 60 ng DNA from plasma. *The x-axis represents different patient groups: 1 (orange) for sepsis patients, 2 (blue) for patients with organ failure, and 3 (green) for control patients. The y-axis in panel (A) shows the detected cGAMP concentration analyzed with ELISA and panel (B) shows the quantified cGAMP per mtDNA. The black lines on the graphs and their respective numbers represent the median value.*

4.4.5.1 Evaluation of uncertainty in cGAMP determination

The ELISA analyses were conducted in duplicates, and the calculated cGAMP concentrations are presented as the average of the two parallels. To evaluate what concentration range of cGAMP was most prone to variation within the duplicates, the relative difference between them was plotted against the average cGAMP concentration in **Figure 4.21**. The EV samples (**Figure 4.21 A**) did not show any correlation between the relative difference and cGAMP concentration. However, the relative uncertainty in determining the cGAMP concentration in the plasma samples appeared to increase with higher cGAMP levels (**Figure 4.21 B**). This suggests that at higher cGAMP concentrations, the ELISA assay may be less precise and more prone to variability. High-concentration samples with low absorbance signals can be more variable due to minor sources of error or noise that can impact final absorbance readings.

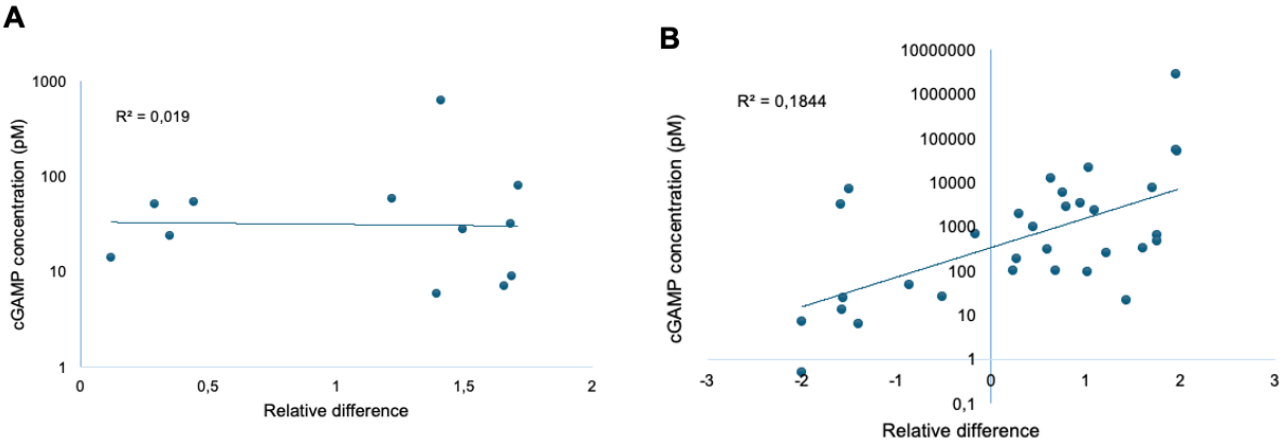

Figure 4.21: Duplicate measurements from EVs and plasma samples presented as A and B, respectively to visualize relationship between the duplicate variation and average cGAMP concentration. *The x-axis displays the relative differences between duplicates, while the y-axis illustrates the average cGAMP concentration of the duplicates of each sample. Panel (A) shows the relative differences in samples using EV DNA, while panel (B) shows the relative differences in samples using plasma DNA.*

4.4.5.2 The contribution of RNA to the activation of cGAS

Based on the MST and ELISA assay results (**Figure 4.6**), it is indicated a strong binding between cGAS and RNA, and showed cGAMP production (**Figure 4.11**). We therefore investigated the effect of removing RNA using a RNase with defined substrate specificity. For our initial approach, we opted for RNaseIf, which is used to remove contaminating RNA from DNA isolates. This enzyme can eliminate ssRNA while leaving RNA-DNA hybrids, dsRNA, and DNA unaffected. We added NEBuffer to the sample, which was then split into two separate tubes. We added RNaseIf to one of the tubes, while the other tube was treated with Milli-Q water to serve as the negative control. Due to limited material availability, the amount of nucleic acids was adjusted to 30 ng, instead of 60 ng as previous optimization suggested. The results from the analysis are presented in **Figure 4.22** and **Figure 4.23**, which show the outcomes from the EV and plasma samples, respectively. The green bars represent the samples without RNase treatment, while the blue bars represent those treated with RNase. In some samples, the absence of blue bars indicates that cGAMP was not detected in the samples treated with RNase. The ELISA analysis showed a decrease in cGAMP levels in RNase-treated samples compared to untreated samples. This confirmes the impact of RNA content on cGAS activation by human DNA samples. This finding further supports the specificity of cGAS binding to RNA observed in the MST assay. The data presented in **Figures 4.22** and **4.23** suggests that RNase treatment is more effective in EV samples than in plasma samples, indicating a higher abundance of free ssRNA within EVs compared to plasma.

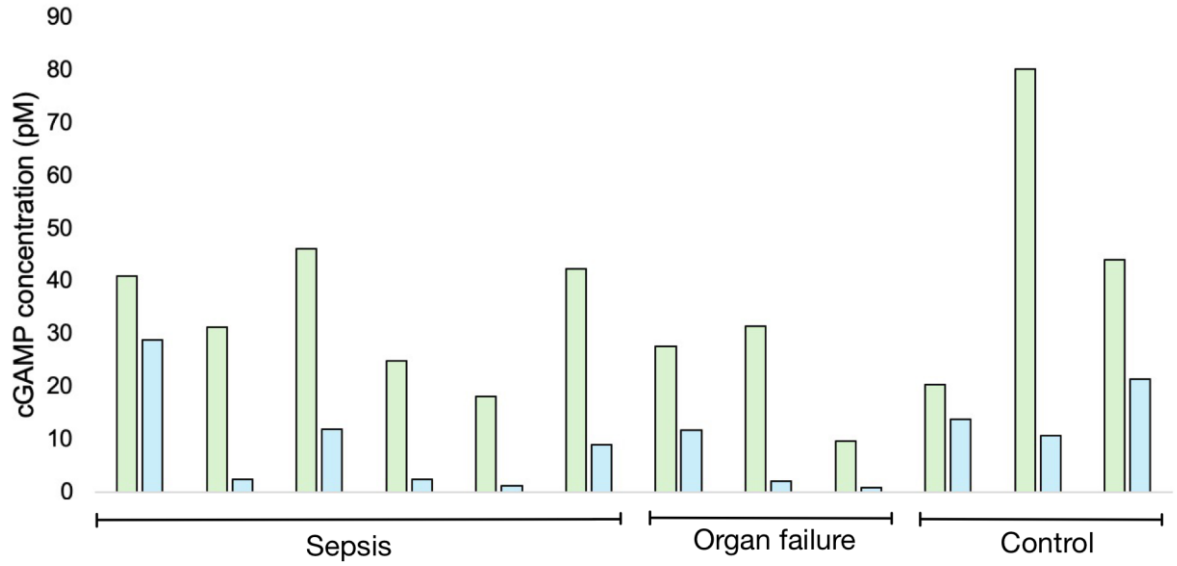

Figure 4.22: Enzymatic activity on RNase-treated human material from EVs. *The x-axis shows the different samples, while the y-axis shows the cGAMP production detected using an ELISA assay. The green bars represent*

the samples without RNase, while the blue bars on the right represent those treated with RNase. 30 ng of DNA was used in each enzyme reaction.

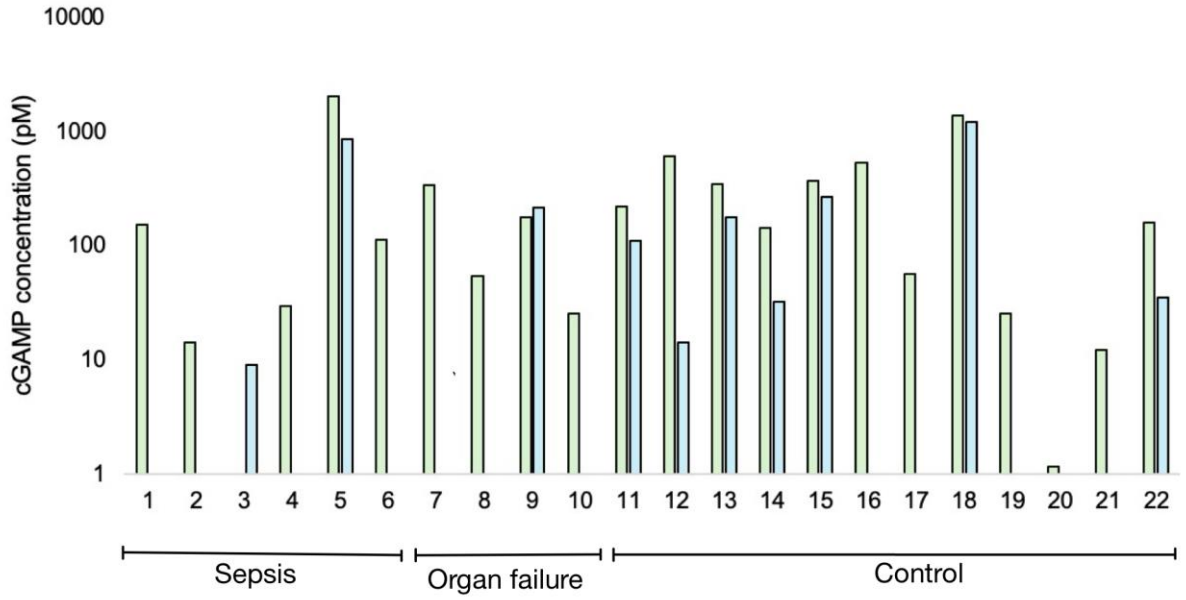

Figure 4.23: Enzymatic activity on RNase-treated human material from plasma samples. *The x-axis shows the different samples, while the y-axis shows the cGAMP production detected using an ELISA assay. The green bars represent the samples without RNase, while the blue bars on the right represent those treated with RNase. 30 ng of DNA was used in each enzyme reaction.*

5 DISCUSSION

This master's thesis has, as a pilot project in understanding the role of mtDNA damage in sepsis, explored the potential of cGAS activation upon circulating DNA in sepsis. The thesis was motivated by studies indicating that elevated levels of mtDNA are associated with a poor prognosis in sepsis (Wang et al., 2020), and that damaged DNA is more effective than intact DNA in activating cGAS (L. Wang et al., 2022). The project involved the expression and purification of cGAS, measurement of its binding affinity, and quantification of cGAMP production to assess enzymatic activity. Samples from patients with sepsis, organ failure, and control groups were analyzed to quantify nDNA, mtDNA and mtDNA damage in both EVs and plasma samples. Additionally, cGAS enzymatic activity was measured using patient material as the nucleic acids activating cGAS. The discussion focuses on cGAS protein expression, purification, activation, and challenges related to nucleic acid quantification and ELISA-based cGAMP detection. It also explores the role of cGAS in immune responses and enzymatic activity on patient samples. The findings shed light on the factors influencing cGAS functionality and its implications for various diseases.

5.1 EXPRESSION OF HUMAN CGAS

Due to cost considerations and reproducibility, we produced recombinant cGAS instead of purchasing the commercial cGAS. As shown in **Figure 4.7**, the recombinant cGAS is at least as efficient as the commercial one, if not more efficient. The higher variation in binding affinity also favors the in-house-produced cGAS.

5.1.1 TAGS AND TRIMMING FOR PURIFICATION OF RECOMBINANT CGAS

The expressed cGAS contained a hexa-His-tag which was included to simplify the purification process. The His-tag is a short sequence of histidine residues that enables one-step purification of the recombinant protein through IMAC. The histidine residues in the tag have a strong affinity for metal ions such as nickel, cobalt, or zinc, immobilized on a chromatography matrix. This method is commonly used in biotechnology and structural biology to purify proteins (Young et al., 2012). Furthermore, the His-tag is relatively tiny and has no significant impact on the target protein's structure or function, making it a popular choice for protein purification.

Including a SUMO-tag in fusion proteins expressed in prokaryotic systems, such as *E. Coli*, has enhanced their solubility (Marblestone et al., 2006). This is because the SUMO-tag aids in the protein's proper folding and structural stability, leading to increased production compared to proteins without the tag. Additionally, research has demonstrated that genetically engineered SUMO-based tags can boost protein expression across various cell types. Consequently, the addition of a SUMO-tag has emerged as a widely utilized approach for improving protein solubility and expression in different cellular systems (Young et al., 2012).

A TEV cleavage site in recombinant proteins was included to enable production of cGAS without tags. The TEV protease acts specifically on the amino acid sequence ENLYFQ/G, making it a precise tag removal tool (Raran-Kurussi et al., 2017). It is highly efficient and compatible with a broad range of fusion proteins. Its usage simplifies the purification process and ensures the integrity of the target protein for the following studies.

The vector consists of residues 157-522 of the human cGAS protein. This particular fragment comprises two highly conserved domains: the nucleotidyltransferase core domain (160–330) and the Mab21 domain (213-513) (Wu et al., 2014). To ensure a stable and globular protein, we have excluded the first 156 residues, which are expected to be unstructured and flexible amino acids.

5.1.2 cGAS VARIANTS

After the expression and purification of the 6xHistag-SUMO-cGAS fusion protein, it was divided into two fractions. In one of the fractions, the 6xHis-SUMO-tag was removed by cleaving the TEV cleavage site with a TEV protease. The fusion protein (6xHistag-SUMO-cGAS) from the other fraction and the truncated protein (cGAS) were then stored in two separate ways; one of which was stored on ice, and the other was mixed with glycerol in a 1:1 ratio and stored at -20°C. MST was performed on both variants stored on ice; the results did not show a significant difference. All four variants' enzymatic activity was analyzed by quantifying cGAMP production using ELISA. The results from the ELISA analysis (**Figure 4.9**) did not show a significant difference either, with only about a 5% difference between the most and least efficient cGAS variants. However, the fusion protein mixed with glycerol and stored at -20°C exhibited the highest cGAMP concentration. Adding glycerol to the protein solution induces conformational changes, leading to a more compact and stable state (Ramm et

al., 2021). This has a protective effect on the degradation of the protein. The fusion protein on glycerol at -20°C is the most efficient variant and is additionally stabilized by glycerol. The enzymatic activity of this variant was compared to that of a commercial cGAS, and it was found to be approximately equal (**Figure 4.7**). Hence, this variant was selected for future experiments.

5.1.3 Optimization of factors affecting the cGAS activation

The enzymatic reaction was optimized before analyzing the patient material. The buffer conditions were optimized, resulting in a buffer that contains Zinc since the presence of Zn^{2+} ions in physiological buffers is necessary for cGAS activation (Yu & Liu, 2021). Zn^{2+} induces cGAS phase transition in the presence of DNA, promoting its activation. Furthermore, the amount of nucleic acids in the analysis was optimized by a dilution series (**Figure 4.10**). At around 60 ng of nucleic acids, the increase in cGAMP appears to be reaching maximal detection range. This might be due to reasons like enzyme saturation, where the cGAS enzymes have already been utilized, or product inhibition, where accumulation of cGAMP inhibits the enzymatic activity of cGAS. Additionally, the ELISA assay may become less effective at high analyte concentrations due to factors such as saturation, non-specific binding, or interference. This optimization step led to the decision of using 60 ng of nucleic acids extracted from the patient samples.

5.2 Limitations and challenges in the study

5.2.1 Methods of nucleic acid quantification

The nucleic acids in the samples were quantified using Nanodrop and PicoGreen quantification methods and qPCR. When comparing the results from these methods (**Figure F.1** in Appendix F), they did not correlate, as the Nanodrop showed differences in the concentrations in different samples. In contrast, the PicoGreen intensity indicated more constant concentrations, even CT values (determined by qPCR) showed large variations. The reason is that contaminants and other interfering substances in the samples can influence the measured absorbance from Nanodrop. In contrast, the PicoGreen method is more specific in detecting dsDNA since fluorescence is more sensitive than absorbance. This suggests that the PicoGreen method may be more reliable for accurate quantification of dsDNA. However, we aimed to examine

components that can activate cGAS, which may also include other nucleic acids than dsDNA (see **Figure 4.11**).

The Nanodrop method is not very sensitive at concentrations below 20 ng/µL, and according to this method, the samples with extracted DNA contained around 0.5 to 3.5 ng/µL for both sample types (EV and plasma). On the other hand, the mtDNA CT values from the qPCR analysis indicated that the plasma samples contain significantly higher amounts of mtDNA than the EV samples. The same was discovered with the nDNA CT values. The nDNA levels were too low to be detected in the EV samples. Conversely, the nDNA levels were detectable in the plasma samples (**Figure 4.14**), and surprisingly, there were significantly higher levels of nDNA in the sepsis and organ failure groups compared to the control groups. This may suggest increased occurrences of cell death or other mechanisms that lead to the release of nDNA into the circulation during sepsis and organ failure in these patients, making nDNA a potential biomarker for disease severity or progression. Additionally, plasma may be a more informative sample for analyzing circulating factors, such as nDNA. These varieties means that the difference in nucleic acids in the samples is probably greater than the results from Nanodrop and PicoGreen analyses indicated. This finding suggests that the cGAS enzymatic activity analyses may not have been as accurate as preferred due to the uncertainty of the amount of nucleic acids.

5.2.2 MTDNA DAMAGE ANALYSES

mtDNA damage analysis involves inhibiting the Taq restriction enzyme. This method works on the principle that if the enzyme cannot cut the DNA, the DNA is likely damaged, which means it cannot recognize the specific sequence. However, it is essential to note that mutations may cause enzyme inhibition sometimes, although this is not very common. Therefore, not all enzyme inhibition is necessarily due to DNA damage. It should also be noted that the restriction enzyme mainly cleaves dsDNA but can also cut ssDNA and RNA-DNA hybrids, although less frequently. The DNA damage assay has several strengths, such as directly comparing damage in nDNA and mtDNA, high sensitivity, low sample amounts needed, and gene-specific measurement. However, it has some areas for improvement, including the inability to detect certain types of DNA damage, lack of specific information about the detected damage, regiospecificity affecting accuracy, and limited accuracy in determining mtDNA copy number due to supercoiled mtDNA (Furda et al., 2014).

5.2.3 LIMITATION OF THE ELISA-BASED CGAMP DETECTION

We noticed a noteworthy fluctuation in the values obtained from the plate reader across readings during the ELISA analyses. In response, a standard curve was always included for each run using the provided cGAMP in the kit. This variance underscores the crucial resolution requirement for the spectrophotometer used in our experiments. The instrument's sensitivity becomes critical when detecting subtle changes in absorbance, especially in assays where the analyte concentration covers a broad range. For the cGAMP standards, the high range of cGAMP detected (ranging from <10 to >100 000 pM (**Figure 3.5**)), despite a relatively low difference in absorbance (ranging from ~0.1 to ~1.2), limits the accuracy of the readings. Additionally, using small volumes across all the methods in the project introduces an elevated vulnerability to variations in sample preparations, further emphasizing the importance of precise technique and quality control measures.

5.2.4 FUNCTIONALITY OF PURIFIED PROTEIN

The protein variant selected for studying the enzymatic properties of cGAS was a fusion protein that consisted of a 6xHis-tag, SUMO-tag, and TEV cleavage site, in addition to the cGAS residues. The presence of these tags might impact the functionality of the cGAS enzyme compared to its natural form. Additionally, the first 156 amino acid residues were excluded from the cGAS, which could influence the outcome of various analyses. Using the full-length protein could potentially alter the results of different experiments and thus need to be considered when conducting further studies.

The cGAS variant was combined with glycerol and stored at -20°C. This variant appeared to be at least as efficient as the others, if not more effective when compared to the variants stored on ice without glycerol. However, it is still important to consider if the glycerol may affect the cGAS in ways that would not affect it *in vivo*. It is essential to be aware that adding glycerol to the cGAS variant can change the enzyme's conformation, altering its binding properties and activation, which may impact downstream analyses.

5.3 cGAS BINDS PREFERENTIALLY TO RNA-DNA HYBRID

As interpreted from the MST-based binding affinity studies, we found that cGAS binds preferentially to the RNA-DNA hybrid over DNA duplex and mismatch DNA, and we couldn’t distinguish between the two latter. However, L. Wang et al. (2022) showed that sequence composition, length of DNA, and DNA damage can regulate the cGAS activity and

demonstrated that mismatched DNA had better binding affinity than DNA duplex. Mankan et al. (2014) reported that RNA-DNA hybrids trigger cGAMP production but are less effective than dsDNA. They also found that different nucleic acid configurations impact cGAMP production differently. For example, dsRNA fails to trigger cGAMP production, while ssRNA and ssDNA cause minimal responses compared to the dsDNA and RNA-DNA hybrid.

In contrast to the clear preference for RNA-DNA binding in MST, the cGAMP production upon RNA-DNA binding from ELISA did not show the same tendency. Mankan et al. (2014) discovered that RNA-DNA hybrids and dsDNA interact with cGAS differently compared to dsRNA. Computational models revealed that RNA-DNA hybrids and dsDNA bind similarly in the cleft of cGAS, while dsRNA does not fit this aperture due to its wider helical structure. This structural difference suggests that RNA-DNA hybrids can initiate cGAS activity similarly to dsDNA by inducing similar conformational changes in cGAS activation. This finding can explain why DNA: U-DNA activates cGAS as efficiently as DNA duplex and mismatched DNA (**Figure 4.11**). This thesis found that dsDNA resulted in approximately three times more cGAMP production than RNA-DNA hybrid, which is consistent with the findings of the article.

These differences in the results from the MST and ELISA experiments might be due to variations in the experimental conditions. The ELISA analysis contains ATP, GTP, a buffer containing zinc, and other components that could serve as cofactors and affect the binding interactions between cGAS and the different nucleic acid substrates, contributing to the dissimilarities between the experimental methods. Further investigation is required to determine the binding specificity of cGAS and the impact of different experimental conditions, including the role of various cofactors, on the observed interactions. In this project, we prioritized cGAMP production over MST. Consequently, due to time limitations, we did not obtain results from ssRNA or ssDNA on MST.

5.4 The role of EVs in activating immune responses

EVs are crucial in certain diseases, such as sepsis. Their effects can be positive or negative depending on their origin and content. While they can cause sepsis or systemic inflammatory response syndrome (SIRS), they also have significant therapeutic potential. Recent studies have demonstrated that EVs have critical functional roles in reducing reactive oxygen species, inflammatory cytokines, and chemokines, influencing macrophage polarization and apoptosis,

and increasing anti-inflammatory cytokines (Weber et al., 2023). A study by (Li et al., 2020) revealed that mtDNA in EV exists in higher quantities and longer fragments than the circulating mtDNA. Additionally, this thesis found that damaged mtDNA was more prevalent in EVs than in circulating mtDNA, indicating a possible link between EV cargo and disease. It is essential to understand the role of EVs, including their cargo of mitochondrial DNA, in disease diagnosis, especially in sepsis and other inflammatory conditions.

A recent study by Sansone et al. (2017) has shown the potential of EVs in transferring genetic material to other cells, specifically the complete mitochondrial genome. This process significantly impacts the regulation of metabolism in cancer cells, especially those that are estrogen receptor-positive breast cancer cells. In hormonal therapy-resistant breast cancer, some breast cancer cells have impaired oxidative phosphorylation, but the transfer of mtDNA-enriched EVs from oxidative phosphorylation-proficient cells can reverse the impairment. The potential therapeutic benefits of EVs are not limited to cancer but extend to various diseases, including sepsis. As the research progresses, EVs as therapeutic agents could become more widespread, and their therapeutic potential could be realized in treating a wide range of diseases.

This thesis found that EVs contain more damaged mtDNA than plasma samples. This suggests that EVs may transfer damaged genetic material during cellular communication, which could indicate increased cellular stress. This finding raises questions about the mechanisms managing EV cargo packaging and release and the significance of EV-derived mtDNA in recipient cells. This discovery could provide insights into intercellular signaling and disease mechanisms.

5.5 cGAS ENZYMATIC ACTIVITY MEDIATED BY PATIENT SAMPLES

5.5.1 THE ROLE OF cGAS IN SEPSIS

Based on the results of this project, it has not been proven that cGAS can be hyperactivated by nucleic acids circulating during sepsis. The amount of cGAMP produced with the DNA from the EV samples was not significantly different between the groups. On the other hand, the cGAMP produced using DNA from plasma samples showed results indicating more cGAS activation in the control group compared to the sepsis and organ failure group. This might

suggest that the cGAS pathway is not as critical to sepsis as previously thought and hypothesized and that other immune pathways may be involved in the immune response to sepsis.

The production of cGAMP is significantly different between the samples using DNA from EVs and DNA from plasma. This may be due to differences in the types of nucleic acids in the various sample types. Shen et al. (2023) discovered that cGAS becomes excessively active in sepsis due to the release of mtDNA into the cytosol. This leads to the activation of cGAS signaling, which further worsens the inflammatory response and causes tissue damage. Quantification of mtDNA (**Figures 4.12 and 4.13**) revealed higher levels in the plasma samples compared to the EV samples. In the EV samples, there is no apparent difference between the groups. In the plasma samples, the sepsis patients tend to have lower mtDNA levels than the rest of the plasma groups. The findings in the article of Shen et al. and this thesis both see a linkage between mtDNA and cGAS activation, indicating that this area should be further investigated as a possible biomarker for sepsis.

5.5.2 Correlation between the state of mtDNA and cGAS activation

Even though a higher proportion of damaged mtDNA has been found in EV samples than in plasma samples (as shown in **Figure 4.17 and 4.18**), this damage does not increase cGAMP production. As plasma samples show a higher concentration of cGAMP and EV samples exhibit more significant mtDNA damage, there is no clear correlation between the two. Nonetheless, given the overall higher mtDNA content in plasma samples, the extent of damaged mtDNA may be more comparable between the groups than the results suggest.

5.5.3 The contribution of RNA to cGAS activation

RNase treatment was performed on the samples to investigate the role of RNA in cGAS activation. The RNA-binding activity of cGAS plays a crucial role in modulating its function and activation. While cGAS has been traditionally recognized as a DNA-binding protein, recent evidence suggests that its interaction with various RNA molecules, including transfer RNA, circular RNA, and RNA-DNA hybrids, can influence its activity (Ma et al., 2021). The experiment results showed a decrease in cGAMP production in nearly all RNase-treated

samples, indicating that RNA presence plays a considerable role in cGAS activation and the consequential cGAMP production. The Nanodrop nucleic acid quantification showed clearly higher levels than the PicoGreen method, which only detects dsDNA. Hence, the higher levels detected with Nanodrop may be due to the presence of RNA (single and double-stranded). When quantifying DNA with Nanodrop, the A260/A280 ratio differed from ~1.8 to >2.0, which indicated the presence of RNA in some samples. It is important to note that the RNase used primarily targets ssRNA, and thus, it is possible that RNA-DNA hybrids or dsRNA were still present in the samples. The contribution of RNA to the signal may be more significant than demonstrated and should be further investigated. This analysis was conducted to characterize the nucleic acids in the different patient groups.

6 CONCLUSION AND FUTURE PERSPECTIVES

This study employed MST, ELISA, and qPCR to investigate cGAS binding affinity, cGAMP production, nucleic acid concentration, and quality of circulating DNA, with respect to the potential role of cGAS activation in sepsis. The research found that both DNA and RNA, single and double-stranded could induce cGAMP production by activating cGAS. Isolated DNA from plasma generally resulted in higher cGAS activation than DNA from EV samples. However, the cGAMP production normalized to mtDNA copies showed clearly higher levels with the EVs, especially the sepsis group. Further, the mtDNA damage assay showed that plasma samples contained more mtDNA, whereas the prevalence of damaged mtDNA was higher in the EV samples. These results may indicate a link between mtDNA and cGAS activation, suggesting that damaged mtDNA is potentially more activating.

The thesis also investigated other nucleic acids present in the human material. It was demonstrated that pretreatment with RNaseIf considerably impacted cGAS activation, indicating that the isolated DNA contains a considerable amount of ssRNA, which awards further characterization in sepsis research. In addition, the plasma samples had detectable levels of nDNA, where the sepsis and organ failure groups had considerably higher levels of nDNA than the control group. The EVs did not contain detectable levels of nDNA.

The findings presented in this thesis provide valuable insights that can be used to design a more extensive study based on this pilot project. In this case, the number of participants in each patient group was limited. Therefore, further research is necessary with larger cohorts and broader disease states to confirm preliminary findings and understand the clinical significance of cGAS signaling in human health and disease. Further investigation could yield valuable insights into the mechanisms of cGAS activation and its role in sepsis.

The ELISA analysis was conducted by estimating the amount of DNA based on the Nanodrop measurements. However, as these values might not be exact, it would be beneficial to perform these analyses again using the same quantity of mtDNA measured with qPCR instead. Also, conducting an additional study to quantify cGAS enzymes in different cohorts would be valuable, such as using Western blot to quantify cGAS proteins or qPCR to investigate the cGAS expression. This would be valuable to study in both EVs and plasma samples; however,

analyzing plasma samples may be more beneficial since they provide a more comprehensive view of circulating factors and could help us better understand the bigger picture.

Moreover, the binding specificity of cGAS and the impact of various experimental conditions, including the role of different cofactors, on the observed interactions, require deeper investigation. Exploring the substrates further, including single-stranded substrates and substrates of more than 44 bp, in combination with enzyme-digested patient samples, would be intriguing. Enzymes such as RNAseIf, RNAseH, dsDNase, and ssDNase could be tested. Future research could also focus on examining the therapeutic potential of EVs, including their cargo of mitochondrial DNA, in disease diagnosis, especially in sepsis and other inflammatory conditions. This could lead to the development of more effective diagnostic and therapeutic strategies for sepsis. Finally, further exploration of the role of RNA and other nucleic acids in cGAS activation and the immune response during sepsis, using enzymes like DNase I or Duplex DNase, could provide valuable insights into the complex mechanisms underlying sepsis.

REFERENCES

Anderson, S., Bankier, A. T., Barrell, B. G., de Bruijn, M. H., Coulson, A. R., Drouin, J., Eperon, I. C., Nierlich, D. P., Roe, B. A., Sanger, F., Schreier, P. H., Smith, A. J., Staden, R., & Young, I. G. (1981). Sequence and organization of the human mitochondrial genome. *Nature*, *290*(5806), 457-465. https://doi.org/10.1038/290457a0

Boyapati, R. K., Tamborska, A., Dorward, D. A., & Ho, G. T. (2017). Advances in the understanding of mitochondrial DNA as a pathogenic factor in inflammatory diseases. *F1000Res*, *6*, 169. https://doi.org/10.12688/f1000research.10397.1

Cadet, J., & Wagner, J. R. (2013). DNA base damage by reactive oxygen species, oxidizing agents, and UV radiation. *Cold Spring Harb Perspect Biol*, *5*(2). https://doi.org/10.1101/cshperspect.a012559

Das, U. N. (2023). Infection, Inflammation, and Immunity in Sepsis. *Biomolecules*, *13*(9). https://doi.org/10.3390/biom13091332

Decout, A., Katz, J. D., Venkatraman, S., & Ablasser, A. (2021). The cGAS-STING pathway as a therapeutic target in inflammatory diseases. *Nat Rev Immunol*, *21*(9), 548-569. https://doi.org/10.1038/s41577-021-00524-z

Di Caro, V., Walko, T. D., 3rd, Bola, R. A., Hong, J. D., Pang, D., Hsue, V., Au, A. K., Halstead, E. S., Carcillo, J. A., Clark, R. S., & Aneja, R. K. (2016). Plasma Mitochondrial DNA--a Novel DAMP in Pediatric Sepsis. *Shock*, *45*(5), 506-511. https://doi.org/10.1097/SHK.0000000000000539

Dragan, A. I., Casas-Finet, J. R., Bishop, E. S., Strouse, R. J., Schenerman, M. A., & Geddes, C. D. (2010). Characterization of PicoGreen interaction with dsDNA and the origin of its fluorescence enhancement upon binding. *Biophys J*, *99*(9), 3010-3019. https://doi.org/10.1016/j.bpj.2010.09.012

Fekete, S., Beck, A., Veuthey, J. L., & Guillarme, D. (2014). Theory and practice of size exclusion chromatography for the analysis of protein aggregates. *J Pharm Biomed Anal*, *101*, 161-173. https://doi.org/10.1016/j.jpba.2014.04.011

Ferdous, S., Dopp, J. L., & Reuel, N. F. (2021). Optimization of E. Coli Tip-Sonication for High-Yield Cell-Free Extract using Finite Element Modeling. *AIChE J*, *67*(10). https://doi.org/10.1002/aic.17389

Furda, A., Santos, J. H., Meyer, J. N., & Van Houten, B. (2014). Quantitative PCR-based measurement of nuclear and mitochondrial DNA damage and repair in mammalian cells. *Methods Mol Biol*, *1105*, 419-437. https://doi.org/10.1007/978-1-62703-739-6_31

Gallucci, S., Lolkema, M., & Matzinger, P. (1999). Natural adjuvants: endogenous activators of dendritic cells. *Nat Med*, *5*(11), 1249-1255. https://doi.org/10.1038/15200

Garcia-Martinez, I., Santoro, N., Chen, Y., Hoque, R., Ouyang, X., Caprio, S., Shlomchik, M. J., Coffman, R. L., Candia, A., & Mehal, W. Z. (2016). Hepatocyte mitochondrial DNA drives nonalcoholic steatohepatitis by activation of TLR9. *J Clin Invest*, *126*(3), 859-864. https://doi.org/10.1172/JCI83885

Gauer, R., Forbes, D., & Boyer, N. (2020). Sepsis: Diagnosis and Management. *Am Fam Physician*, *101*(7), 409-418. https://www.ncbi.nlm.nih.gov/pubmed/32227831

Giles, R. E., Blanc, H., Cann, H. M., & Wallace, D. C. (1980). Maternal inheritance of human mitochondrial DNA. *Proc Natl Acad Sci U S A*, *77*(11), 6715-6719. https://doi.org/10.1073/pnas.77.11.6715

Gomes, L., Monteiro, G., & Mergulhao, F. (2020). The Impact of IPTG Induction on Plasmid Stability and Heterologous Protein Expression by Escherichia coli Biofilms. *Int J Mol Sci*, *21*(2). https://doi.org/10.3390/ijms21020576

Gustot, T. (2011). Multiple organ failure in sepsis: prognosis and role of systemic inflammatory response. *Curr Opin Crit Care*, *17*(2), 153-159. https://doi.org/10.1097/MCC.0b013e328344b446

Habbane, M., Montoya, J., Rhouda, T., Sbaoui, Y., Radallah, D., & Emperador, S. (2021). Human Mitochondrial DNA: Particularities and Diseases. *Biomedicines*, *9*(10). https://doi.org/10.3390/biomedicines9101364

He, Z., Tan, J. S., Lai, O. M., & Ariff, A. B. (2015). Optimization of conditions for the single step IMAC purification of miraculin from Synsepalum dulcificum. *Food Chem*, *181*, 19-24. https://doi.org/10.1016/j.foodchem.2014.11.166

Herzner, A. M., Hagmann, C. A., Goldeck, M., Wolter, S., Kubler, K., Wittmann, S., Gramberg, T., Andreeva, L., Hopfner, K. P., Mertens, C., Zillinger, T., Jin, T., Xiao, T. S., Bartok, E., Coch, C., Ackermann, D., Hornung, V., Ludwig, J., Barchet, W., . . . Schlee, M. (2015). Sequence-specific activation of the DNA sensor cGAS by Y-form DNA structures as found in primary HIV-1 cDNA. *Nat Immunol*, *16*(10), 1025-1033. https://doi.org/10.1038/ni.3267

Hu, Y. W., Zhang, J., Wu, X. M., Cao, L., Nie, P., & Chang, M. X. (2018). TANK-Binding Kinase 1 (TBK1) Isoforms Negatively Regulate Type I Interferon Induction by Inhibiting TBK1-IRF3 Interaction and IRF3 Phosphorylation. *Front Immunol*, *9*, 84. https://doi.org/10.3389/fimmu.2018.00084

Hunter, M. P., Ismail, N., Zhang, X., Aguda, B. D., Lee, E. J., Yu, L., Xiao, T., Schafer, J., Lee, M. L., Schmittgen, T. D., Nana-Sinkam, S. P., Jarjoura, D., & Marsh, C. B. (2008). Detection of microRNA expression in human peripheral blood microvesicles. *PLoS One*, *3*(11), e3694. https://doi.org/10.1371/journal.pone.0003694

Jerabek-Willemsen, M., Wienken, C. J., Braun, D., Baaske, P., & Duhr, S. (2011). Molecular interaction studies using microscale thermophoresis. *Assay Drug Dev Technol*, *9*(4), 342-353. https://doi.org/10.1089/adt.2011.0380

Kaczmarek, A., Vandenabeele, P., & Krysko, D. V. (2013). Necroptosis: the release of damage-associated molecular patterns and its physiological relevance. *Immunity*, *38*(2), 209-223. https://doi.org/10.1016/j.immuni.2013.02.003

Kahlert, C., & Kalluri, R. (2013). Exosomes in tumor microenvironment influence cancer progression and metastasis. *J Mol Med (Berl)*, *91*(4), 431-437. https://doi.org/10.1007/s00109-013-1020-6

Kahlert, C., Melo, S. A., Protopopov, A., Tang, J., Seth, S., Koch, M., Zhang, J., Weitz, J., Chin, L., Futreal, A., & Kalluri, R. (2014). Identification of double-stranded genomic DNA spanning all chromosomes with mutated KRAS and p53 DNA in the serum exosomes of patients with pancreatic cancer. *J Biol Chem*, *289*(7), 3869-3875. https://doi.org/10.1074/jbc.C113.532267

Kalluri, R. (2016). The biology and function of exosomes in cancer. *J Clin Invest*, *126*(4), 1208-1215. https://doi.org/10.1172/JCI81135

Kim, J., Kim, H. S., & Chung, J. H. (2023). Molecular mechanisms of mitochondrial DNA release and activation of the cGAS-STING pathway. *Exp Mol Med*, *55*(3), 510-519. https://doi.org/10.1038/s12276-023-00965-7

Kowal, J., Arras, G., Colombo, M., Jouve, M., Morath, J. P., Primdal-Bengtson, B., Dingli, F., Loew, D., Tkach, M., & Thery, C. (2016). Proteomic comparison defines novel markers to

characterize heterogeneous populations of extracellular vesicle subtypes. *Proc Natl Acad Sci U S A*, *113*(8), E968-977. https://doi.org/10.1073/pnas.1521230113

Krychtiuk, K. A., Ruhittel, S., Hohensinner, P. J., Koller, L., Kaun, C., Lenz, M., Bauer, B., Wutzlhofer, L., Draxler, D. F., Maurer, G., Huber, K., Wojta, J., Heinz, G., Niessner, A., & Speidl, W. S. (2015). Mitochondrial DNA and Toll-Like Receptor-9 Are Associated With Mortality in Critically Ill Patients. *Crit Care Med*, *43*(12), 2633-2641. https://doi.org/10.1097/CCM.0000000000001311

Lazo, S., Noren Hooten, N., Green, J., Eitan, E., Mode, N. A., Liu, Q. R., Zonderman, A. B., Ezike, N., Mattson, M. P., Ghosh, P., & Evans, M. K. (2021). Mitochondrial DNA in extracellular vesicles declines with age. *Aging Cell*, *20*(1), e13283. https://doi.org/10.1111/acel.13283

Li, X., Shu, C., Yi, G., Chaton, C. T., Shelton, C. L., Diao, J., Zuo, X., Kao, C. C., Herr, A. B., & Li, P. (2013). Cyclic GMP-AMP synthase is activated by double-stranded DNA-induced oligomerization. *Immunity*, *39*(6), 1019-1031. https://doi.org/10.1016/j.immuni.2013.10.019

Li, Y., Guo, X., Guo, S., Wang, Y., Chen, L., Liu, Y., Jia, M., An, J., Tao, K., & Xing, J. (2020). Next generation sequencing-based analysis of mitochondrial DNA characteristics in plasma extracellular vesicles of patients with hepatocellular carcinoma. *Oncol Lett*, *20*(3), 2820-2828. https://doi.org/10.3892/ol.2020.11831

Liu, S., Cai, X., Wu, J., Cong, Q., Chen, X., Li, T., Du, F., Ren, J., Wu, Y. T., Grishin, N. V., & Chen, Z. J. (2015). Phosphorylation of innate immune adaptor proteins MAVS, STING, and TRIF induces IRF3 activation. *Science*, *347*(6227), aaa2630. https://doi.org/10.1126/science.aaa2630

Liu, V., Escobar, G. J., Greene, J. D., Soule, J., Whippy, A., Angus, D. C., & Iwashyna, T. J. (2014). Hospital deaths in patients with sepsis from 2 independent cohorts. *JAMA*, *312*(1), 90-92. https://doi.org/10.1001/jama.2014.5804

Luecke, S., Holleufer, A., Christensen, M. H., Jonsson, K. L., Boni, G. A., Sorensen, L. K., Johannsen, M., Jakobsen, M. R., Hartmann, R., & Paludan, S. R. (2017). cGAS is activated by DNA in a length-dependent manner. *EMBO Rep*, *18*(10), 1707-1715. https://doi.org/10.15252/embr.201744017

Ma, Y., Wang, X., Luo, W., Xiao, J., Song, X., Wang, Y., Shuai, H., Ren, Z., & Wang, Y. (2021). Roles of Emerging RNA-Binding Activity of cGAS in Innate Antiviral Response. *Front Immunol*, *12*, 741599. https://doi.org/10.3389/fimmu.2021.741599

Man, S. M., & Kanneganti, T. D. (2016). Converging roles of caspases in inflammasome activation, cell death and innate immunity. *Nat Rev Immunol*, *16*(1), 7-21. https://doi.org/10.1038/nri.2015.7

Mankan, A. K., Schmidt, T., Chauhan, D., Goldeck, M., Honing, K., Gaidt, M., Kubarenko, A. V., Andreeva, L., Hopfner, K. P., & Hornung, V. (2014). Cytosolic RNA:DNA hybrids activate the cGAS-STING axis. *EMBO J*, *33*(24), 2937-2946. https://doi.org/10.15252/embj.201488726

Marblestone, J. G., Edavettal, S. C., Lim, Y., Lim, P., Zuo, X., & Butt, T. R. (2006). Comparison of SUMO fusion technology with traditional gene fusion systems: enhanced expression and solubility with SUMO. *Protein Sci*, *15*(1), 182-189. https://doi.org/10.1110/ps.051812706

Medzhitov, R. (2008). Origin and physiological roles of inflammation. *Nature*, *454*(7203), 428-435. https://doi.org/10.1038/nature07201

Morelli, A. E., Larregina, A. T., Shufesky, W. J., Sullivan, M. L., Stolz, D. B., Papworth, G. D., Zahorchak, A. F., Logar, A. J., Wang, Z., Watkins, S. C., Falo, L. D., Jr., & Thomson, A. W. (2004). Endocytosis, intracellular sorting, and processing of exosomes by dendritic cells. *Blood*, *104*(10), 3257-3266. https://doi.org/10.1182/blood-2004-03-0824

Nakahira, K., Haspel, J. A., Rathinam, V. A., Lee, S. J., Dolinay, T., Lam, H. C., Englert, J. A., Rabinovitch, M., Cernadas, M., Kim, H. P., Fitzgerald, K. A., Ryter, S. W., & Choi, A. M. (2011). Autophagy proteins regulate innate immune responses by inhibiting the release of mitochondrial DNA mediated by the NALP3 inflammasome. *Nat Immunol*, *12*(3), 222-230. https://doi.org/10.1038/ni.1980

Nowakowski, A. B., Wobig, W. J., & Petering, D. H. (2014). Native SDS-PAGE: high resolution electrophoretic separation of proteins with retention of native properties including bound metal ions. *Metallomics*, *6*(5), 1068-1078. https://doi.org/10.1039/c4mt00033a

Park-Sarge, O. K., & Sarge, K. D. (2009). Detection of sumoylated proteins. *Methods Mol Biol*, *464*, 255-265. https://doi.org/10.1007/978-1-60327-461-6_14

Picca, A., Guerra, F., Calvani, R., Romano, R., Coelho-Junior, H. J., Damiano, F. P., Bucci, C., & Marzetti, E. (2022). Circulating Mitochondrial DNA and Inter-Organelle Contact Sites in Aging and Associated Conditions. *Cells*, *11*(4). https://doi.org/10.3390/cells11040675

Porat, A., Bhutta, B. S., & Kesler, S. (2024). Urosepsis. In *StatPearls*. https://www.ncbi.nlm.nih.gov/pubmed/29493969

Ramm, I., Sanchez-Fernandez, A., Choi, J., Lang, C., Fransson, J., Schagerlof, H., Wahlgren, M., & Nilsson, L. (2021). The Impact of Glycerol on an Affibody Conformation and Its Correlation to Chemical Degradation. *Pharmaceutics*, *13*(11). https://doi.org/10.3390/pharmaceutics13111853

Raran-Kurussi, S., Cherry, S., Zhang, D., & Waugh, D. S. (2017). Removal of Affinity Tags with TEV Protease. *Methods Mol Biol*, *1586*, 221-230. https://doi.org/10.1007/978-1-4939-6887-9_14

Real, J. M., Ferreira, L. R. P., Esteves, G. H., Koyama, F. C., Dias, M. V. S., Bezerra-Neto, J. E., Cunha-Neto, E., Machado, F. R., Salomao, R., & Azevedo, L. C. P. (2018). Exosomes from patients with septic shock convey miRNAs related to inflammation and cell cycle regulation: new signaling pathways in sepsis? *Crit Care*, *22*(1), 68. https://doi.org/10.1186/s13054-018-2003-3

Sansone, P., Savini, C., Kurelac, I., Chang, Q., Amato, L. B., Strillacci, A., Stepanova, A., Iommarini, L., Mastroleo, C., Daly, L., Galkin, A., Thakur, B. K., Soplop, N., Uryu, K., Hoshino, A., Norton, L., Bonafe, M., Cricca, M., Gasparre, G., . . . Bromberg, J. (2017). Packaging and transfer of mitochondrial DNA via exosomes regulate escape from dormancy in hormonal therapy-resistant breast cancer. *Proc Natl Acad Sci U S A*, *114*(43), E9066-E9075. https://doi.org/10.1073/pnas.1704862114

Sarnecka, A. K., Nawrat, D., Piwowar, M., Ligeza, J., Swadzba, J., & Wojcik, P. (2019). DNA extraction from FFPE tissue samples - a comparison of three procedures. *Contemp Oncol (Pozn)*, *23*(1), 52-58. https://doi.org/10.5114/wo.2019.83875

Shen, X., Sun, C., Cheng, Y., Ma, D., Sun, Y., Lin, Y., Zhao, Y., Yang, M., Jing, W., Cui, X., & Han, L. (2023). cGAS Mediates Inflammation by Polarizing Macrophages to M1 Phenotype via the mTORC1 Pathway. *J Immunol*, *210*(8), 1098-1107. https://doi.org/10.4049/jimmunol.2200351

Singer, M., Deutschman, C. S., Seymour, C. W., Shankar-Hari, M., Annane, D., Bauer, M., Bellomo, R., Bernard, G. R., Chiche, J. D., Coopersmith, C. M., Hotchkiss, R. S., Levy, M. M., Marshall, J. C., Martin, G. S., Opal, S. M., Rubenfeld, G. D., van der Poll, T., Vincent,

J. L., & Angus, D. C. (2016). The Third International Consensus Definitions for Sepsis and Septic Shock (Sepsis-3). *JAMA*, *315*(8), 801-810. https://doi.org/10.1001/jama.2016.0287

Sun, L., Wu, J., Du, F., Chen, X., & Chen, Z. J. (2013). Cyclic GMP-AMP synthase is a cytosolic DNA sensor that activates the type I interferon pathway. *Science*, *339*(6121), 786-791. https://doi.org/10.1126/science.1232458

Sursal, T., Stearns-Kurosawa, D. J., Itagaki, K., Oh, S. Y., Sun, S., Kurosawa, S., & Hauser, C. J. (2013). Plasma bacterial and mitochondrial DNA distinguish bacterial sepsis from sterile systemic inflammatory response syndrome and quantify inflammatory tissue injury in nonhuman primates. *Shock*, *39*(1), 55-62. https://doi.org/10.1097/SHK.0b013e318276f4ca

Timmermans, K., Kox, M., Scheffer, G. J., & Pickkers, P. (2016). Plasma Nuclear and Mitochondrial DNA Levels, and Markers of Inflammation, Shock, and Organ Damage in Patients with Septic Shock. *Shock*, *45*(6), 607-612. https://doi.org/10.1097/SHK.0000000000000549

Vagner, T., Chin, A., Mariscal, J., Bannykh, S., Engman, D. M., & Di Vizio, D. (2019). Protein Composition Reflects Extracellular Vesicle Heterogeneity. *Proteomics*, *19*(8), e1800167. https://doi.org/10.1002/pmic.201800167

Wallace, D. C., & Chalkia, D. (2013). Mitochondrial DNA genetics and the heteroplasmy conundrum in evolution and disease. *Cold Spring Harb Perspect Biol*, *5*(11), a021220. https://doi.org/10.1101/cshperspect.a021220

Wang, D., Zhao, H., Shen, Y., & Chen, Q. (2022). A Variety of Nucleic Acid Species Are Sensed by cGAS, Implications for Its Diverse Functions. *Front Immunol*, *13*, 826880. https://doi.org/10.3389/fimmu.2022.826880

Wang, L., Li, S., Wang, K., Wang, N., Liu, Q., Sun, Z., Wang, L., Wang, L., Liu, Q., Song, C., Liu, C., & Yang, Q. (2022). DNA mechanical flexibility controls DNA potential to activate cGAS-mediated immune surveillance. *Nat Commun*, *13*(1), 7107. https://doi.org/10.1038/s41467-022-34858-6

Wang, L., Zhou, W., Wang, K., He, S., & Chen, Y. (2020). Predictive value of circulating plasma mitochondrial DNA for Sepsis in the emergency department: observational study based on the Sepsis-3 definition. *BMC Emerg Med*, *20*(1), 25. https://doi.org/10.1186/s12873-020-00320-3

Wang, W., Esbensen, Y., Scheffler, K., & Eide, L. (2015). Analysis of mitochondrial DNA and RNA integrity by a real-time qPCR-based method. *Methods Mol Biol*, *1264*, 97-106. https://doi.org/10.1007/978-1-4939-2257-4_10

Weber, B., Henrich, D., Hildebrand, F., Marzi, I., & Leppik, L. (2023). The Roles of Extracellular Vesicles in Sepsis and Systemic Inflammatory Response Syndrome. *Shock*, *59*(2), 161-172. https://doi.org/10.1097/SHK.0000000000002010

West, A. P., & Shadel, G. S. (2017). Mitochondrial DNA in innate immune responses and inflammatory pathology. *Nat Rev Immunol*, *17*(6), 363-375. https://doi.org/10.1038/nri.2017.21

Wu, X., Wu, F. H., Wang, X., Wang, L., Siedow, J. N., Zhang, W., & Pei, Z. M. (2014). Molecular evolutionary and structural analysis of the cytosolic DNA sensor cGAS and STING. *Nucleic Acids Res*, *42*(13), 8243-8257. https://doi.org/10.1093/nar/gku569

Yanez-Mo, M., Siljander, P. R., Andreu, Z., Zavec, A. B., Borras, F. E., Buzas, E. I., Buzas, K., Casal, E., Cappello, F., Carvalho, J., Colas, E., Cordeiro-da Silva, A., Fais, S., Falcon-Perez, J. M., Ghobrial, I. M., Giebel, B., Gimona, M., Graner, M., Gursel, I., . . . De Wever, O. (2015).

Biological properties of extracellular vesicles and their physiological functions. *J Extracell Vesicles*, *4*, 27066. https://doi.org/10.3402/jev.v4.27066

Young, C. L., Britton, Z. T., & Robinson, A. S. (2012). Recombinant protein expression and purification: a comprehensive review of affinity tags and microbial applications. *Biotechnol J*, *7*(5), 620-634. https://doi.org/10.1002/biot.201100155

Yu, L., & Liu, P. (2021). Cytosolic DNA sensing by cGAS: regulation, function, and human diseases. *Signal Transduct Target Ther*, *6*(1), 170. https://doi.org/10.1038/s41392-021-00554-y

Zhou, J., Zhuang, Z., Li, J., & Feng, Z. (2023). Significance of the cGAS-STING Pathway in Health and Disease. *Int J Mol Sci*, *24*(17). https://doi.org/10.3390/ijms241713316

Zhou, W., Whiteley, A. T., de Oliveira Mann, C. C., Morehouse, B. R., Nowak, R. P., Fischer, E. S., Gray, N. S., Mekalanos, J. J., & Kranzusch, P. J. (2018). Structure of the Human cGAS-DNA Complex Reveals Enhanced Control of Immune Surveillance. *Cell*, *174*(2), 300-311 e311. https://doi.org/10.1016/j.cell.2018.06.026

APPENDIX

APPENDIX A: HUMAN MATERIAL

Table A.1: Overview of EV samples from patients with sepsis and organ failure.

Sample	Information
205	Sepsis
903	Sepsis
714	Sepsis
265	Sepsis
565	Sepsis
324	Sepsis
756	Organ failure
702	Organ failure
614	Organ failure

Table A.2: Overview of EV samples from patients of the control group.

Sample	Information
D1	Healthy control
D2	Healthy control
D3	Healthy control

Table A.3: Overview of plasma samples from patients with sepsis and organ failure.

Sample	Information
S046	Sepsis
S087	Sepsis
S712	Sepsis
S714	Sepsis
S725	Sepsis
S767	Sepsis
S771	Sepsis
S820	Sepsis
S059	Organ failure
S115	Organ failure
S238	Organ failure
S268	Organ failure

Table A.4: Overview of plasma samples from patients of the control group. *The fasted individuals had been fasting for 12 hours.*

Sample	Information
20.	Fasted
21.	Fasted
23.	Fasted
24.	Fasted
25.	Fasted
29.	Fasted
30.	Fasted
123.	Non-fasted

124.	Non-fasted
125.	Non-fasted
126.	Non-fasted
127.	Non-fasted
128.	Non-fasted
129.	Non-fasted
132.	Rare metabolic disorders
133.	Rare metabolic disorders
135.	Rare metabolic disorders
136.	Rare metabolic disorders

APPENDIX B: BUFFERS

Buffer A	***Concentration***
NaCl	300 Mm
TRIS pH 8	50 mM
Imidazole	10 mM

Buffer B	***Concentration***
NaCl	300 Mm
TRIS pH 8	50 mM
Imidazole	50 mM

Buffer C	***Concentration***
NaCl	300 Mm
TRIS pH 8	50 mM
Imidazole	300 mM

Coomassie staining solution	***%***
Coomassie blue	0.1%
Acetic acid	10 %
Methanol	40 %

LB-medium	***Gram/Liter***
LB broth	25g
Milli-Q water	1L

Destaining solution	***%***
Glycerol	4 %
Acetic acid	10 %
Methanol	40 %

Buffer D	***Concentration/%***
$MgCl_2$	5 mM
Brij-35	0.01%
DMSO	1 %

Buffer E	***Concentration***
Tris pH 7.5	500 mM
NaCl	1.5 M
$MgCl_2$	100 mM
Zinc	2 mM
Tween	0.10 %

APPENDIX C: OLIGONUCLEOTIDES

Table C.1: Overview of the different Oligonucleotides used in this project and their respective sequences. The oligonucleotides colored in green are fluorescently labeled.

Oligo name	Oligonucleotide	Sequence (5'->3')
Ctrl ISD-F_um	DNA 1	AATTTTTTTTCCACCTTGAAACTTTTCTTTTTCCATTGAAAAAT
Ctrl ISD-F	DNA 2	AATTTTTTTTCCACCTTGAAACTTTTCTTTTTCCATTGAAAAAT
Ctrl ISD-R	DNA 3	ATTTTTCAATGGAAAAAGAAAAGTTTCAAGGTGGAAAAAAAATT
AP ISD-R	DNA 4	ATTTTTCAATGGAAAAAGAAAA(Spd)TTTCAAGGTGGAAAAAAAATT
Mis ISD-R	DNA 5	ATTTTTCAATGGAAAAAGAAAACTTTCAAGGTGGAAAAAAAATT
Ctrl ISR-R	DNA 6	A(U)(U)(U)(U)(U)CAA(U)GGAAAAAGAAAAG(U)(U)(U)CAAGG(U)GGAAAAAAAA(U)(U)
Ctrl ISRNA	RNA 1	AAUUUUUUUUCCACCUUGAAACUUUUCUUUUUCCAUUGAAAAAU
CtrlRNA ISR-R	RNA 2	AUUUUUCAAUGGAAAAAGAAAAGUUUCAAGGUGGAAAAAAAAUU

Table C.2: Overview of the oligonucleotides used in each duplex for the MST and ELISA experiments.

	Double-stranded oligonucleotide	Oligonucleotides combined
MST		
	DNA duplex	DNA 2 + DNA 3
	mismatch DNA	DNA 2 + DNA 5
	RNA-DNA hybrid	DNA 3 + RNA 1
ELISA		
	DNA duplex	DNA 1 + DNA 3
	mismatch DNA	DNA 1 + DNA 5
	RNA-DNA hybrid	DNA 1 + RNA 2
	DNA-uDNA	DNA 1 + DNA 6
	apDNA	DNA 1 + DNA 4
	ssDNA	DNA 1
	ssRNA	RNA 2

APPENDIX D: cGAS BINDING ASSAY

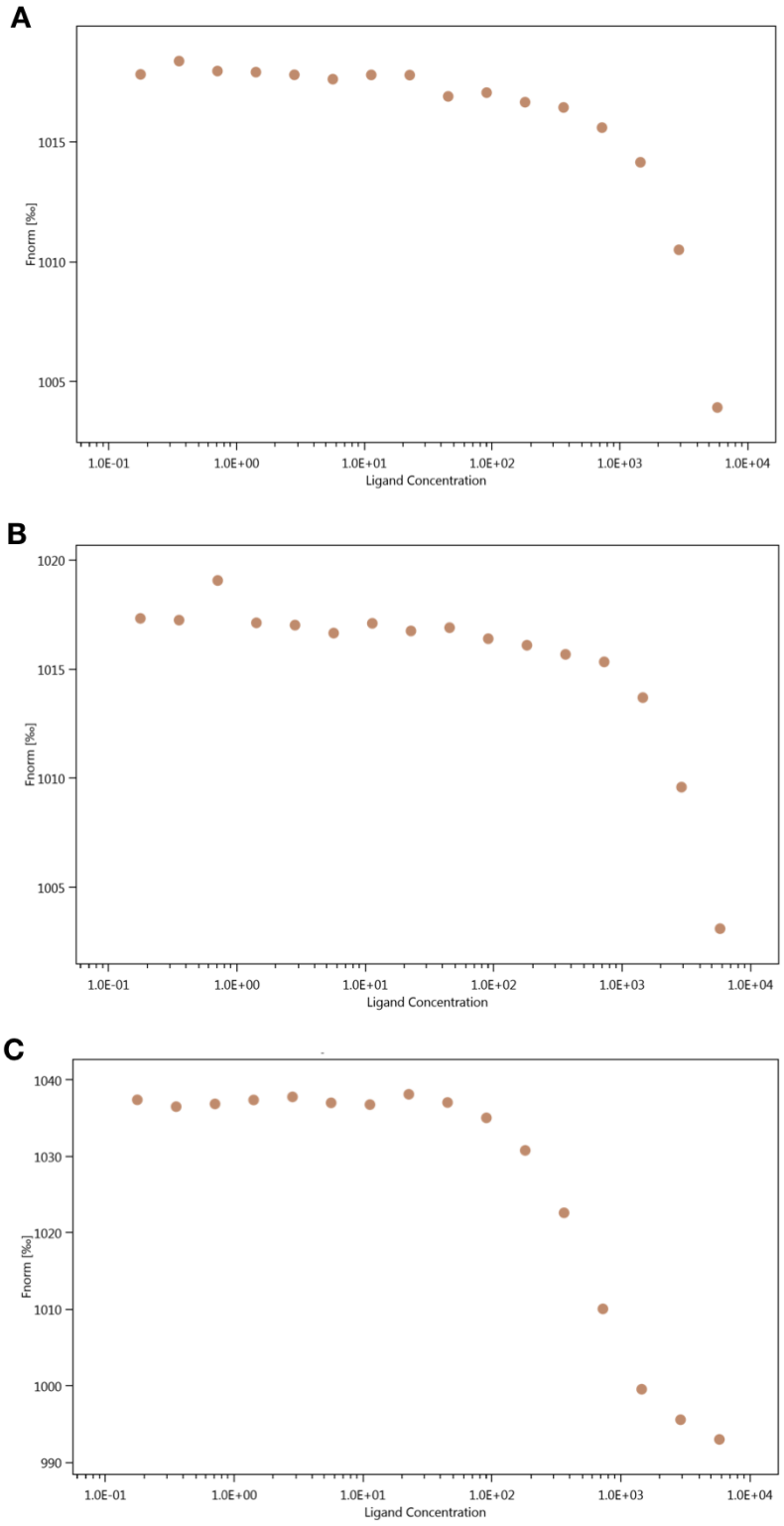

Figure D.1: Dose response from analyzing binding affinity with Microscale Thermophoresis, using the 6xHistag-SUMO-cGAS fusion protein. *The graphs display the normalized change of fluorescence (‰) plotted against the ligand concentration (nM) for three different scenarios: (**A**) DNA duplex, (**B**) DNA with a mismatch, and (**C**) RNA-DNA hybrid.*

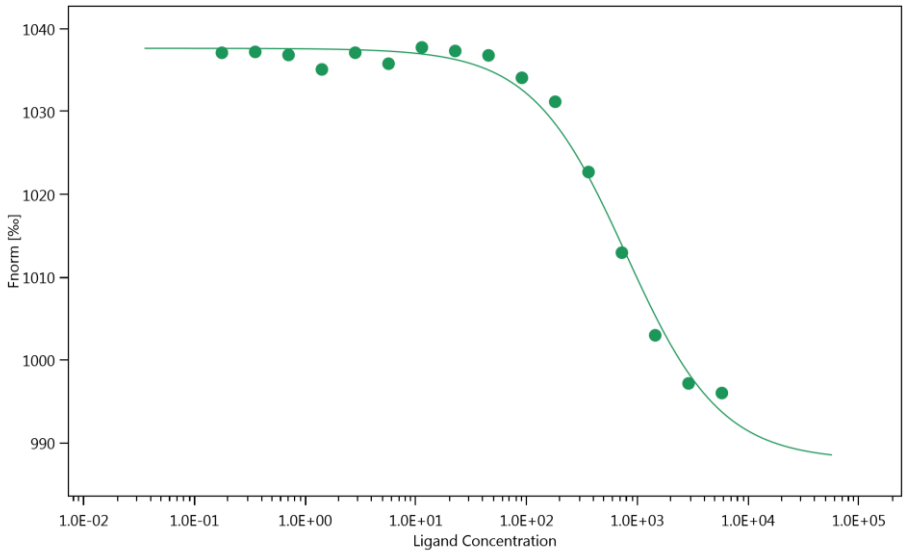

Figure D.2: Dose-response curve obtained from the MST analysis using mismatched DNA and the truncated variant of cGAS.

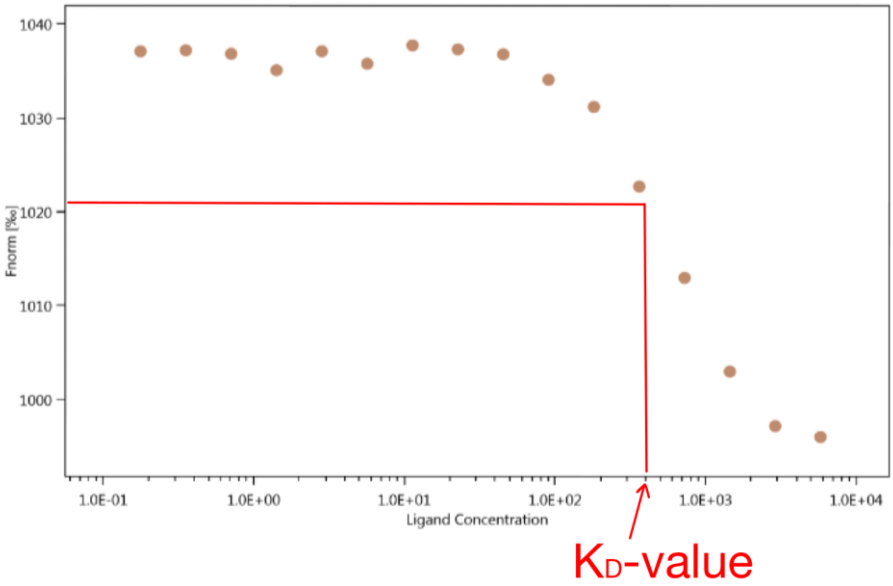

Figure D.3: Illustration defining the K_D-value, where 50% of the protein and oligonucleotides are bound. *The figure shows the binding analysis between cGAS and RNA-DNA hybrid.*

APPENDIX E: cGAS ENZYMATIC ACTIVITY

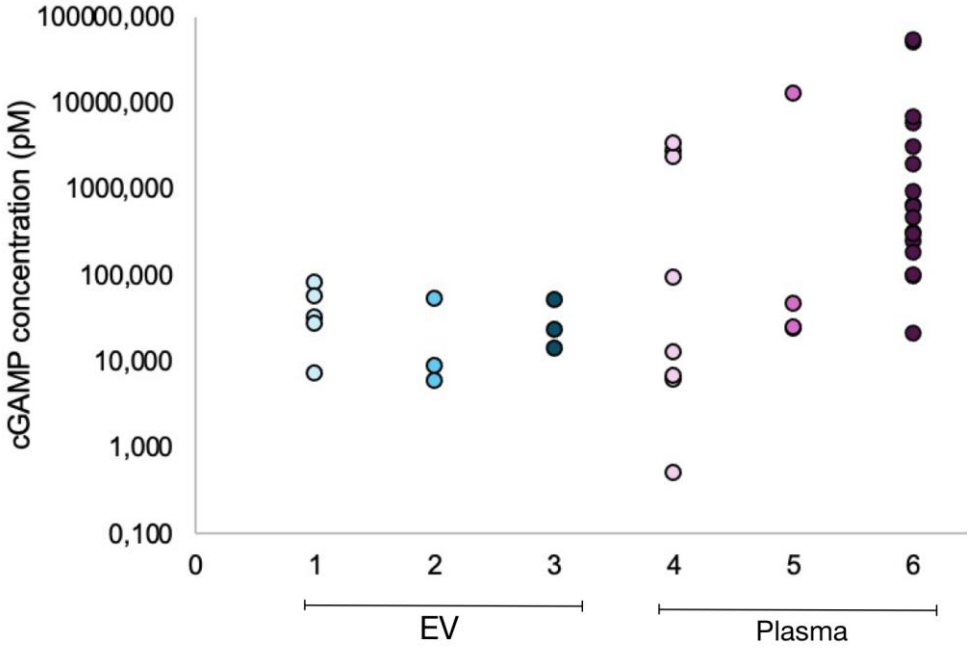

Figure E.1: cGAMP concentration detected using ELISA. *Blue dots (row 1-3) are cGAMP concentrations from EV samples, 1 is sepsis patients, 2 is organ failure, 3 is non-sepsis patients. Purple dots (row 4-6) are cGAMP concentrations from plasma samples, 4 is sepsis patients, 5 is organ failure, 6 is non-sepsis patients.*

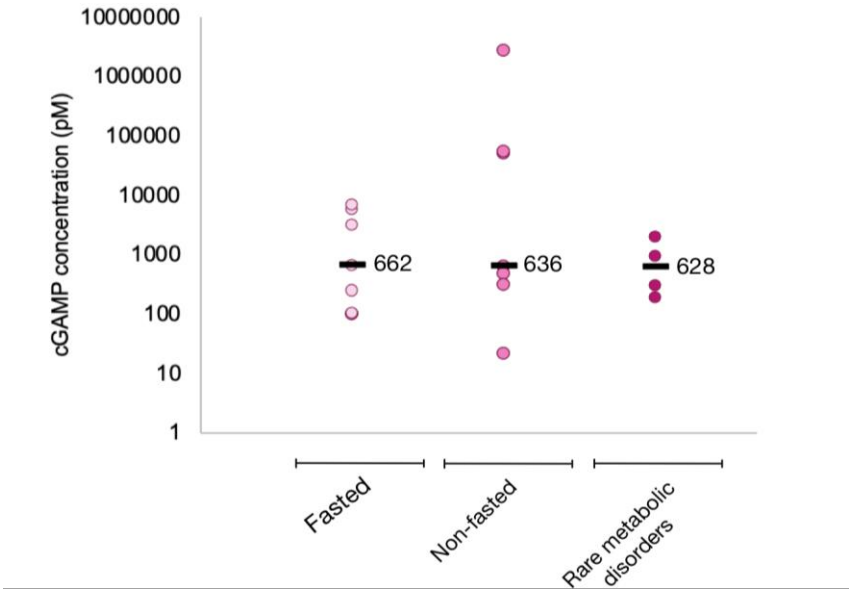

Figure E.2: Comparison of the cGAMP production in the separate plasma sample control groups. *Median values are represented by black lines and their respective numbers within the specific groups.*

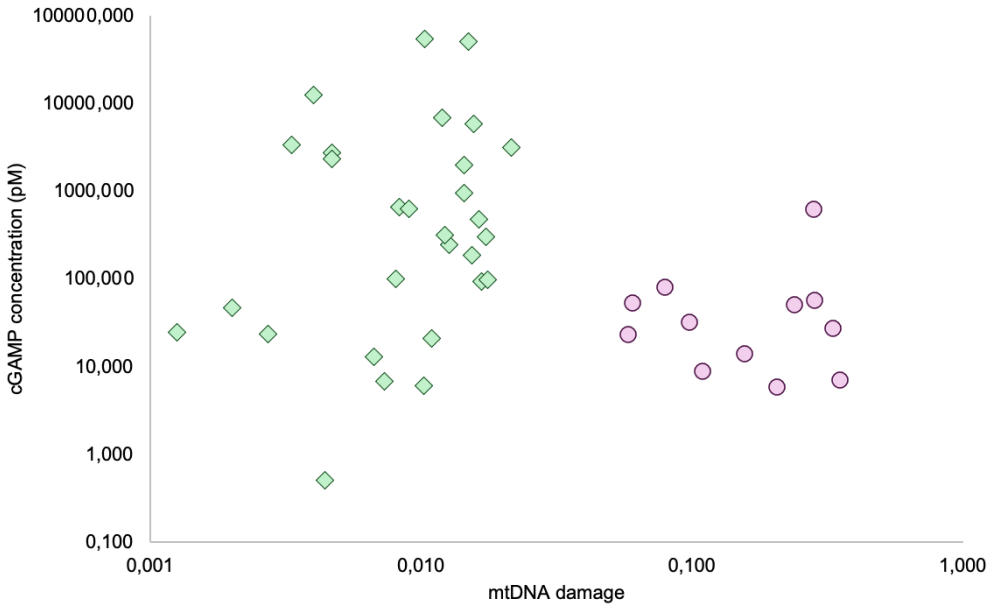

Figure E.3: mtDNA damage vs. detected cGAMP concentration in EVs and plasma samples. *Purple circles represent the EV samples, and green squares show the plasma samples. The x-axis shows the mtDNA damage in each sample, quantified with qPCR, while the y-axis shows the cGAMP concentration quantified with ELISA.*

APPENDIX F: NUCLEIC ACID QUANTIFICATION

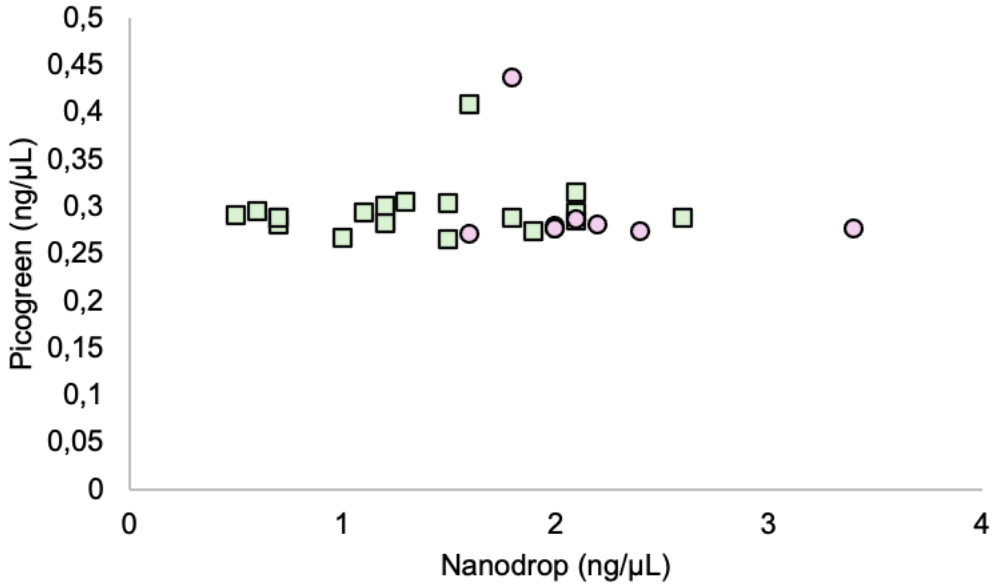

Figure F.1: Comparison between nucleic acid concentration measured with Nanodrop and PicoGreen. *Purple circles are EV DNA from patients (sepsis or organ failure) patients while green squares show the plasma DNA from the control groups.* Both the Nanodrop and PicoGreen values are presented as ng/µL.

Norges miljø- og biovitenskapelige universitet
Noregs miljø- og biovitskapelege universitet
Norwegian University of Life Sciences

Postboks 5003
NO-1432 Ås
Norway